# Integrated network pharmacology and serum metabolomics to reveal the protective mechanism of methanolic extract of BaiYangJie on cisplatin-induced acute kidney injury in mice

BIN XIA[1,2*], JIANGLONG CHEN[1,2*], JINHUI WANG[2,3], DALONG LI[3], LIXIA ZHANG[2,4], JING SU[2,4], XUAN DING[2,4], YANA LV[2,4], SHIFANG LIU[2,4], XUE ZHANG[1,2], TIANZHEN WAN[1,2] and GUANG LI[2,3]

[1]School of Pharmacy, Heilongjiang University of Chinese Medicine, Haerbin, Heilongjiang 150006, P.R. China; [2]Pharmacology Center, Chinese Academy of Medical Sciences and Peking Union Medical College Institute of Medicinal Plant Development Yunnan Branch, Jinghong, Yunnan 666100, P.R. China; [3]Key Laboratory of Biology and Genetic Improvement of Horticulture Crops (Northeast Region), Ministry of Agriculture and Rural Affairs, School of Horticulture and Landscape Architecture, Northeast Agricultural University, Harbin, Heilongjiang, 150006, P.R. China; [4]Yunnan Key Laboratory of Southern Medicine Utilization, Institute of Medicinal Plant Development, Chinese Academy of Medical Sciences & Peking Union Medical College, Jinghong, Yunnan 666100, P.R. China

Received November 11, 2025; Accepted April 28, 2026

DOI: 10.3892/etm.2026.13199

**Abstract.** Cisplatin, a chemotherapeutic drug, produces severe nephrotoxicity and at present, there are no effective drugs to clinically prevent or treat it. In the Dai nationality, BaiYangJie is used to treat poisoning caused by chemicals or drugs. Previous research has demonstrated that the methanolic extract of BaiYangJie (MEAG) can treat cisplatin-induced nephrotoxicity; however, its mechanism of action remains unclear. The aim of the present study was therefore to identify the potential mechanism of action of MEAG in cisplatin nephrotoxicity using a combination of network pharmacology and serum metabolomics. Initially, network pharmacology analysis was used to identify hub targets and signalling pathways involved in the renoprotective effects of MEAG. Subsequently, plasma metabolomics profiling utilising ultra performance liquid chromatography-quadrupole time-of-flight mass spectrometry technology revealed key metabolic alterations and pathway modulations associated with MEAG treatment. Finally, integrated analysis uncovered key molecular mechanisms, which were subsequently validated by western blotting and immunohistochemistry. A total of 13 endogenous metabolites were identified in serum metabolomics, primarily involved in phenylalanine metabolism and in the biosynthesis of phenylalanine, tyrosine and tryptophan. The treatment of MEAG in cis-induced acute kidney injury primarily involved regulating the inflammatory response, responses to lipid and chemical stress, the FoxO signalling pathway, arachidonic acid metabolism and the NF-κB signalling pathway. Animal experiments showed that MEAG can inhibit inflammation and the expression of the migration inhibitory factor (MIF)/NF-κB pathway. Through integrated network pharmacological analysis, metabolomic profiling and experimental validation, it was systematically elucidated that MEAG exerted its therapeutic effects through dual regulatory mechanisms: Suppressing inflammatory responses by inhibiting overactivation of the MIF/NF-κB signalling pathway and restoring phenylalanine metabolic homeostasis. These findings thus provide a mechanistic foundation for developing targeted therapeutic strategies against chemotherapy-associated nephrotoxicity.

*Correspondence to:* Dr Guang Li, Pharmacology Center, Chinese Academy of Medical Sciences and Peking Union Medical College Institute of Medicinal Plant Development Yunnan Branch, 138 Xuanwei Avenue, Yunjinghong Street, Xishuangbanna, Jinghong, Yunnan 666100, P.R. China
E-mail: lhbg311@hotmail.com

*Contributed equally

*Abbreviations:* AKI, acute kidney injury; BUN, blood urea nitrogen; CMC-Na, sodium carboxymethyl cellulose; GO, Gene Ontology; IDA, Information Dependent Acquisition; KEGG, Kyoto Encyclopaedia of Genes and Genomes; MEAG, methanolic extract of BaiYangJie; MIF, migration inhibitory factor; Scr, serum creatinine

*Key words:* network pharmacology, metabolomics, cisplatin, acute kidney injury, migration inhibitory factor, NF-κB, phenylalanine metabolism

## Introduction

Acute kidney injury (AKI) is a clinical syndrome characterised by a rapid decline in kidney function over a short period of time. AKI remains a major global health burden, with recent evidence showing that it affects millions of individuals worldwide each year and is associated with high mortality and an increased risk of progression to chronic kidney disease. Therefore, AKI has become an important public health problem requiring early prevention and effective therapeutic strategies (1). Pathogenic factors for AKI include hypovolemia, septic shock, nephrotoxic drug use and urinary

tract obstruction (2), among which 12.2% of AKI cases are associated with the use of nephrotoxic therapeutics (3).

Cisplatin (Cis) is widely used to treat a number of solid cancer types, including lung, ovarian, testicular, bladder, and head and neck cancer. However, owing to its side effects, particularly nephrotoxicity, its clinical application is limited. Cis-induced acute kidney injury (Cis-AKI), which is characterised by renal tubular injury, inflammation and impaired renal function, occurs in 20-30% of treated patients despite hydration-based preventive measures. Identifying effective drugs for treating kidney injury and elucidating their mechanisms of action therefore remains a challenge (4-6). However, owing to its side effects, including nephrotoxicity, ototoxicity, hepatotoxicity, gastrointestinal toxicity and neurotoxicity, its clinical application is markedly limited, especially due to Cis nephrotoxicity, as patients with tumours often suffer from Cis-induced AKI (Cis-AKI), which is characterised by acute tubular necrosis and inflammation, with an incidence rate as high as 20-30% (7). Identifying effective drugs for treating kidney injury and elucidating their mechanisms of action therefore remains a challenge (8).

BaiYangJie is the dry whole grass of *Arundina graminifolia* (D. Don) Hochr. (*Laeli*, *Arundina Blume*), whose primary active chemical components are stilbenes, phenanthrene and flavonoids, which exhibit anti-inflammatory, antioxidant, antibacterial and antitumour activities (9). BaiYangJie is a characteristic medicine of the Dai nationality and is used to treat urinary system diseases, including urinary tract infections and chemical, pharmaceutical and food-induced poisoning, including liver and kidney detoxification (9). Previously, it has been found that the methanolic extract of BaiYangJie (MEAG) can improve Cis-AKI (10). Despite this discovery, the mechanism by which MEAG improves Cis-AKI remains unclear, hindering its clinical application. Therefore, it is necessary to further explore its mechanisms of action.

Metabolomics has the unique potential to identify biomarkers that predict the incidence, severity and progression of diseases, including disease-related endogenous metabolites and metabolic signatures, and to reveal perturbed metabolic pathways, thereby providing novel clues to mechanistic abnormalities (11). Therefore, metabolomics is often used to study botanical drugs in complex situations (12). Both tools account for the complexity of biological systems and can complement each other, which is beneficial for the systematic study of diseases with complex mechanisms. Consequently, network pharmacology was combined with serum metabolomics to comprehensively examine how MEAG affects Cis-AKI in mice, providing a theoretical basis for the future development of anti-renal injury drugs.

## Materials and methods

*Drugs and reagents. Arundina graminifolia* (D. Don) Hochr samples used in the present study were collected from the Yunnan Branch of the Institute of Medicinal Plant Development (Chinese Academy of Medical Sciences, Jinghong, China). It was identified as *Arundina graminifolia* (D. Don) Hochr. by Research Professor Lixia Zhang (Yunnan Branch of the Institute of Medicinal Plant Development, Chinese Academy of Medical Sciences, Jinghong, China). The appraisal report is shown in Fig. S1.

The following reagents were used in the present study: Resveratrol (cat. no. 111535; National Institutes for Food and Drug Control), pterostilbene (cat. no. 455753; J&K Chemical Ltd.), acetonitrile [American Chemical Society/high-performance liquid chromatography (HPLC) grade; cat. no. AH015-4HC; Honeywell International Inc.], methanol (HPLC grade; cat. no. 01104351; Adamas-Beta® Ltd.), formic acid (HPLC grade; cat. no. F112034; Shanghai Aladdin Biochemical Technology Co., Ltd.), distilled water [Watsons Water; AS Watson Group (HK) Ltd.], Cis (cat. no. 275688; J&K Chemical Ltd.), H&E (cat. no. G1120) and Masson staining kit (cat. no. G1346; both from Beijing Solarbio Science & Technology Co., Ltd.), kidney injury molecule 1 (KIM-1)/hepatitis A virus cellular receptor 1 rabbit polyclonal antibody (cat. no. 30948-1-AP) and lipocalin-2/neutrophil gelatinase-associated lipocalin (NGAL) rabbit polyclonal antibody (cat. no. 30700-1-AP; discontinued; both from ProteinTech Group, Inc.), mouse IL-6 (cat. no. YJ063159), IL-1β (cat. no. YJ35346) and TNF-α (cat. no. YJ002095) ELISA kits (all from Shanghai Yuanju Bio-Technology Co., Ltd.) migration inhibitory factor (MIF) recombinant rabbit monoclonal antibody (cat. no. ET1703-89; HUABIO), MIF rabbit monoclonal antibody (cat. no. A22623; ABclonal, Inc.), phosphorylated (p)-NF-κB rabbit polyclonal antibody (cat. no. WL02169), IL-6 (cat. no. WL02841), IL-1β (cat. no. WL02257) and TNF-α rabbit polyclonal antibody (cat. no. WL01581; all from Wanleibio Co., Ltd.), S-vision polymer secondary antibody for immunohistochemistry (IHC; goat anti-rabbit; cat. no. G1302; Wuhan Servicebio Technology Co., Ltd.), sodium citrate antigen retrieval buffer (cat. no. G1219-1L; Wuhan Servicebio Technology Co., Ltd.), anti-NF-κB p65 rabbit polyclonal antibody (cat. no. GB11997-100; Wuhan Servicebio Technology Co., Ltd.), HRP-conjugated β-actin recombinant rabbit monoclonal antibody (cat. no. PSH03-63; HUABIO) and HRP-conjugated goat anti-rabbit IgG polyclonal antibody (cat. no. HA1001; HUABIO).

*Preparation of extract*

*Preparation of MEAG freeze-dried powder.* A total of 100 g BaiYangJie powder was added to 1,000 ml methanol and treated ultrasonically (800 W; 40 kHz; 25±3˚C) for 30 min, filtered and concentrated under reduced pressure. The concentrated solution was stored overnight at -80˚C, then freeze-dried to a powder (pro-4055/4085 freeze-dryer; Nanjing Genscience Instrument and Equipment Co., Ltd.) and stored at 4˚C. A total of 20 mg freeze-dried methanol extract powder was added to a 100 ml volumetric flask and methanol was added to make up the volume to 100 ml. Then, the mixture was sonicated and finally filtered through a 0.22 $\mu$m microporous membrane for further analyses.

*Preparation of the reference substance.* A total of ~1 mg resveratrol and pterostilbene were added to 100 ml volumetric flasks. Methanol was added to dilute to scale and make up a total volume of 100 ml to obtain a 10 $\mu$g/ml standard solution. This solution was filtered through a 0.22 $\mu$m microporous membrane for further analysis.

*Establishment of Cis-AKI in a mouse model.* All animal experiments were approved by the Institutional Ethics Review Committee of the Yunnan Branch of the Institute of Medicinal Plant Development, Chinese Academy of Medical Sciences

(Jinghong, China; approval no. 20240213001). The present study was strictly performed in accordance with the guidelines of the National Research Council Guide for the Care and Use of Laboratory Animals (13). Male Kunming (KM) mice [weight: 20-22 g; aged 8 weeks; Sibefu (Beijing) Biotechnology Co., Ltd.] were housed in SPF environments with a controlled temperature (22±2˚C), relative humidity (50±5%), atmospheric pressure (101±2 kPa) and a 12-h light/dark cycle, before being allowed to acclimatise for 7 days, during which animals were provided with *ad libitum* access to water and standardised feed. A total of 30 KM mice were randomly allocated into three experimental cohorts (n=10/group): i) Nor [0.5% sodium carboxymethyl cellulose (CMC-Na), intragastrically], ii) Cis (Cis 13 mg/kg, intraperitoneally) and iii) MEAG (800 mg/kg, intragastrically). The MEAG cohort received daily oral gavage for 10 consecutive days, while the mice in the Nor group were given equivalent volumes of 0.5% CMC-Na solution (0.1 ml/10 g). On day 7, Cis-induced nephropathy was established in the Cis through a single intraperitoneal dose (13 mg/kg). Biological specimens (blood and kidney tissues) were collected on day 10. Mice were anaesthetised with 4% isoflurane in an induction chamber until loss of consciousness and then maintained at a concentration of 1-3% using a mask. Once the toe pinch reflex disappeared for >60 sec, breathing became deep and slow and there was no limb contraction or respiratory change upon strong pinching, the head was fixed and the jugular vein was gently compressed to engorge. A capillary tube was inserted into the inner canthus of the eye to collect blood, with the volume reaching 20-30% of the total blood volume (0.5-0.8 ml for 25 g mice). Immediately after blood collection, euthanasia was performed (under deep anaesthesia, rapid cervical dislocation), To clarify, cervical dislocation rather than exsanguination (blood loss) was used for euthanasia as waiting for natural mortality due to blood loss was prohibited. Mortality was determined when breathing and heartbeat stopped for ≥2 min and the pupils dilated and fixed. The left kidney was collected and fixed in 4% paraformaldehyde at 24˚C for 24 h for histopathological examination, while the right kidney was rapidly frozen in liquid nitrogen and stored at -80˚C for molecular biological experiments.

*Metabolomics sample preparation*. Serum aliquots (80 µl) were mixed with 320 µl methanol/acetonitrile (ACN) solution (1:1; v/v) followed by 30 sec vortex-mixing. The mixture underwent cryoprecipitation at -20˚C for 60 min. Subsequent centrifugation (4˚C; 16,100 x g; 15 min) yielded supernatant that was lyophilised using the Bionoon-VAC1 vacuum concentrator (Shanghai Bionoon Biotechnology Co., Ltd.) at 4˚C. The lyophilised products were reconstituted in 160 µl ACN/water (1:1; v/v) solution. Quality control (QC) samples were prepared by pooling 10 µl aliquots from each reconstituted sample. Prior to analysis, all specimens were filtered through 0.22 µm membrane filters to remove particulate matter.

*Ultra-performance liquid chromatography-quadrupole time-of-flight mass spectrometry (UPLC-Q-TOF-MS) analysis*. Chromatographic separation was achieved using an Acquity HSS T3 column (2.1x100.0 mm; 1.8 µm; Waters China Ltd.) on a Shimadzu LC400 system (Shimadzu Scientific Instruments) coupled with AB SCIEX X500B Q-TOF mass spectrometer (SCIEX) operating in dual electrospray ionization mode. The eluent system comprised of (A) 0.1% aqueous formic acid and (B) 0.1% formic acid in acetonitrile. The following parameters were used: Flow rate, 0.3 ml/min; column oven, 35˚C; injection volume, 5 µl; nitrogen gas temperature, 350˚C; and nitrogen nebuliser flow rate, 10 l/min. Mass detection employed information-dependent acquisition mode with the following settings: Primary MS spectrometry scan, m/z 100-1,200; and secondary tandem MS scan, m/z 50-1,200. The top 15 intense ions were selected for fragmentation.

For the MEAG samples, the mobile phase gradient was 0-2 min, 5% B; 2-5 min, 5-20% B; 5-8 min, 20-40% B; 8-10 min, 40-60% B; 10-15 min, 60-100% B; 15-19 min, 100% B; 19-20 min, 100-5% B; and 20-23 min, 5% B. Nitrogen gas was used in each gas path and ionisation voltage was 5,500 V. Sprayer pressure was 60 psi, the auxiliary heating gas was 60 psi, the air curtain gas was 35 psi, the cone hole voltage was 100 V and the collision energy was 10 V.

For the metabolomics samples, the mobile phase gradient was 0-2 min, 5% B; 2-8 min, 5-50% B; 8-12 min, 50-80% B; 12-14 min, 80-95% B; 14-17 min, 95% B; 17-18 min, 95-5% B; and 18-21 min, 5% B. Nitrogen gas was used in each gas path. The ionisation voltage was 4,500 V, the sprayer pressure was 60 psi, the auxiliary heating gas was 60 psi, the air curtain gas was 35 psi, the cone hole voltage was 80 V and the collision energy was 20 V.

*Network pharmacology and molecular docking*. Active components were initially screened using SwissADME (http://www.swissadme.ch) with dual criteria: Oral bioavailability ≥30% and drug-likeness. Potential therapeutic targets were identified through SwissTargetPrediction (swisstargetprediction.ch). Cis-AKI targets were systematically retrieved from five major databases: Online Mendelian Inheritance in Man (OMIM; https://omim.org/), DrugBank (version 5.1.10; https://go.drugbank.com/), GeneCards (version 5.22; https://www.genecards.org/), Therapeutic Target Database (TTD; https://db.idrblab.net/ttd/; accessed on October 31, 2023) and DisGeNET (version 24.0; https://www.disgenet.org/). The targets shared by MEAG components and Cis-AKI were identified using the Venn analysis module in SRplot (bioinformatics.com.cn).

Protein-protein interaction (PPI) networks were constructed using Search Tool for the Retrieval of Interacting Genes/Proteins (STRING; version 11.5; https://cn.string-db.org/), with species restricted to *Homo sapiens* and a confidence cutoff >0.4. Following network visualisation in Cytoscape (14) (version 3.7.1), the 'CytoNCA' plugin (version 2.4.6) was used to prioritise nodes based on multidimensional centrality metrics: Degree, betweenness and closeness. A network of 12 metabolites was constructed using the Search Tool For Interactions Of Chemicals (https://stitch-db.org/) and Cytoscape to represent the metabolic module regulated by MEAG. The consensus targets underwent comprehensive functional annotation using Kyoto Encyclopedia of Genes and Genomes (KEGG) (15,16) pathways and Gene Ontology (GO) enrichment analyses in Metascape (metascape.org), with organism specification restricted to *Homo sapiens*. Based on the number of gene enrichments, diagrams were drawn using SRplot.

*Metabolomics data analyses*. Original data for each sample were processed to obtain peak alignment, peak extraction, peak comparison and standardisation using MS DIAL software (version 4.9.221218) as previously described (17). The online MetaboAnalyst (version 6.0; https://www.metaboanalyst.ca/) database was used for principal component analysis (PCA) and orthogonal partial least squares discriminant analysis (OPLS-DA). By analysing differences between the Nor group and Cis group and between the Cis group and MEAG group, differential metabolites [variable importance in the projection (VIP)>1; P<0.05] were identified and imported into MetaboAnalyst for enrichment and metabolic pathway analyses.

*Renal function tests and histological examination*. Serum creatinine (Scr) and blood urea nitrogen (BUN) concentrations were quantified using the SMT-120VP clinical chemistry system (Chengdu Seamaty Technology Co., Ltd.) with a seven-parameter renal function assay kit (cat. no. AW03076; Chengdu Seamaty Technology Co., Ltd.), according to the manufacturer's protocol.

Kidney specimens were fixed in 4% paraformaldehyde at 24˚C for 24 h, followed by sequential dehydration at room temperature and paraffin embedding at 60˚C for 2 h. Subsequently, 4 $\mu$m microtome sections were prepared. A total of three tissue slices per sample were deparaffinized with xylene at room temperature for 15 min twice, rehydrated through a graded ethanol series at room temperature and rinsed with distilled water. For H&E staining, the sections were stained with haematoxylin at room temperature for 5 min, rinsed with running tap water, differentiated, blued and then counterstained with eosin at room temperature for 2 min. For Masson's trichrome staining, the sections were stained according to the manufacturer's protocol. Briefly, the sections were stained with haematoxylin at room temperature for 5 min, stained with Masson's ponceau acid fuchsin solution at room temperature for 5 min, differentiated with phosphomolybdic acid solution at room temperature for 2 min and counterstained with aniline blue solution at room temperature for 2 min. After staining, all sections were dehydrated, cleared and mounted with neutral resin. Renal morphological alterations were visualised using an Olympus BX53 bright-field microscope at x200 and x400 magnification (Olympus Corporation). The glomerular architecture, proximal convoluted tubule morphology, basement membrane characteristics of glomeruli and collagen deposition patterns were observed.

*ELISA*. Circulating concentrations of TNF-α, IL-1β and IL-6 in mouse serum were quantified using commercially available ELISA kits for mice according to the manufacturer's protocols.

*IHC*. Following dewaxing, the sections were rehydrated through a graded ethanol series and rinsed with PBS. Antigen retrieval was performed by boiling samples in sodium citrate antigen retrieval buffer at 100˚C for 10 min. Subsequently, tissues were treated with a quenching reagent (3% hydrogen peroxide solution) at room temperature for 5 min to block endogenous peroxidase activity, followed by blocking with 10% goat serum (Wuhan Servicebio Technology Co., Ltd.) for 60 min at room temperature. The goat serum was discarded and KIM-1 rabbit polyclonal antibody (1:300), NGAL rabbit polyclonal antibody (1:200) and MIF rabbit monoclonal antibody (1:800) were applied to the sections and incubated overnight (~12 h) at 4˚C. Next, secondary antibody conjugation was performed using S-vision polymer secondary antibody for IHC at room temperature for 60 min before the sections were washed three times with PBS. Signals were visualised using diaminobenzidine at room temperature for 3 min, counterstained with haematoxylin at room temperature for 1 min, dehydrated through a graded ethanol series, cleared with xylene and mounted. Tissues were viewed using standard bright-field illumination.

*Western blotting*. Renal tissues were homogenised in lysis buffer (cat. no. CW2333; CoWin Biosciences, Inc.) supplemented with 1% protease/phosphatase inhibitors, followed by a 1 h incubation to ensure complete lysis and subsequent centrifugation (16,100 x g; 20 min; 4˚C). Protein quantification was performed using a BCA protein detection kit (cat. no. CW0014; CoWin Biosciences, Inc.). To resolve proteins, a 10% SDS-PAGE gel was used and 30 $\mu$g of protein was loaded per lane before electrophoresis; the resolved proteins were transferred to PVDF membranes. Membranes were blocked with 5% non-fat milk/TBST (at 25˚C for 2 h; 0.05% Tween-20) prior to overnight incubation (4˚C) with anti-MIF (1:1,000), anti-p-NF-κB (1:2,000), NF-κB (1:1,000) anti-IL-6 (1:2,000), anti-IL-1β (1:2,000) and anti-TNF-α (1:2,000). After three TBST washes, membranes were incubated with an HRP-conjugated secondary antibody (25˚C for 2 h; 1:50,000). with β-actin as the internal reference. Signals were visualised with ECL reagents (New Cell & Molecular Biotech Co., Ltd.) and band intensities were quantified using an imaging system from Tanon Science and Technology Co., Ltd. with Image ProPlus (version 5.0; Media Cybernetics, Inc.; https://www.mediacy.com/).

*Statistical analysis*. Statistical analysis was performed utilising GraphPad Prism (version 9.0; Dotmatics) software. Data were compared using a one-way ANOVA followed by Tukey's HSD post hoc test. A total of three independent biological replicates were performed for each experiment. Results are presented as the mean ± SD. P<0.05 was considered to indicate a statistically significant difference.

## Results

*Characterisation of chemical constituents of MEAG*. Based on UPLC-Q-TOF-MS analysis, combined with database searches, reference compounds and related literature, 33 chemical components were identified in MEAG using multi-level MS information (18-24). The chemical components of the MEAG are listed in Table I and the base peak chromatograms of the positive and negative ion modes are shown in Fig. 1A and B.

*Network pharmacology*. A total of 14 active ingredients (Table SI) and 348 active ingredient targets were screened using the Swiss ADME and Swiss Target Prediction databases. A total of 2,514 non-redundant disease targets were retrieved from OMIM, DrugBank, GeneCards, TTD and DisGeNET. A

Table I. Characterisation of main components of MEAG in positive and negative ion modes.

| No. | Compound name | RT, min | Measured value, m/z | Molecular formula | MS/MS | Ion species | Error, ppm |
|---|---|---|---|---|---|---|---|
| 1 | Betaine | 0.826 | 118.0860 | $C_5H_{11}NO_2$ | 58.0649, 118.0862 | $(M^+ H)^+$ | -2.2 |
| 2 | Naringin | 5.411 | 603.1691 | $C_{27}H_{32}O_{14}$ | 603.1686, 441.1173, 409.0927, 277.0471 | $(M^+ Na)^+$ | 1.1 |
| 3 | Verbenalin | 5.502 | 411.1266 | $C_{17}H_{24}O_{10}$ | 411.1272, 249.0751, 231.0647, 187.0754, 181.0507 | $(M^+ Na)^+$ | 1.0 |
| 4 | Riboflavin | 5.934 | 377.1459 | $C_{17}H_{20}N_4O_6$ | 377.1465, 359.1345, 243.0879, 198.0663, 172.0869 | $(M^+ H)^+$ | 0.9 |
| 5 | Mauritianin | 6.439 | 763.2061 | $C_{33}H_{40}O_{19}$ | 763.2036, 617.1505, 477.1587, 331.1008 | $(M^+ Na)^+$ | 0.7 |
| 6 | Rutin | 6.653/ 6.665 | 611.1614/ 609.1451 | $C_{27}H_{30}O_{16}$ | 611.1623, 303.0502, 287.0548, 257.0437, 229.0945/ 609.1424, 300.0253, 271.0233, 255.0288, 178.9980, 151.0031 | $(M^+ H)^+$/ $(M^- H)^-$ | 1.2/-1.7 |
| 7 | Vicenin 2 | 6.899 | 617.1489 | $C_{27}H_{30}O_{15}$ | 617.1476, 471.0946, 455.1299, 331.1005 | $(M^+ Na)^+$ | 2.0 |
| 8 | Isoorientin | 7.111 | 471.0909 | $C_{21}H_{20}O_{11}$ | 471.0905, 309.0374, 185.0425, 147.0453 | $(M^+ Na)^+$ | 2.4 |
| 9 | Kaempferol-4'-glucoside | 7.253 | 471.0908 | $C_{21}H_{20}O_{11}$ | 471.0894, 405.0513, 365.1428, 309.0380, 202.0515, 185.0427 | $(M^+ Na)^+$ | 2.2 |
| 10 | Nepitrin | 7.340 | 479.1193 | $C_{22}H_{22}O_{12}$ | 479.1555, 317.0659, 302.0427, 385.0400, 165.0197, 153.0188 | $(M^+ H)^+$ | 1.9 |
| 11 | Isorhamnetin-3-O-glucoside | 7.340/ 7.366 | 501.1009/ 477.1029 | $C_{22}H_{22}O_{12}$ | 501.1001, 435.0493, 357.0457, 3338.0415, 261.0492, 185.0422/ 477.1020, 314.0415, 299.0191, 285.0395, 271.0236 | $(M^+ Na)^+$/ $(M^- H)^-$ | 1.1/-2.0 |
| 12 | Resveratrol | 8.255 | 229.0859 | $C_{14}H_{12}O_3$ | 229.0876, 211.0768, 183.0811, 193.0643, 109.0279 | $(M^+ H)^+$ | -0.1 |
| 13 | Quercetin | 9.074/ 9.086 | 303.0501/ 301.0350 | $C_{15}H_{10}O_7$ | 303.0506, 285.0398, 257.0450, 247.0602, 229.0500, 153.0191/ 301.0345, 273.0405, 245.0459, 178.9982, 151.0035, 121.0292 | $(M^+ H)^+$/ $(M^- H)^-$ | 0.6/-1.3 |
| 14 | Benzaldehyde | 9.505 | 107.0489 | $C_7H_6O$ | 107.0495, 77.0385 | $(M^+ H)^+$ | -2.2 |
| 15 | Lusianthridin | 9.631 | 243.1013 | $C_{15}H_{14}O_3$ | 243.1016, 228.0783, 215.1074, 211.0756, 197.0967, 181.0651 | $(M^+ H)^+$ | -1.1 |
| 16 | Kaempferol | 9.883 | 287.0547 | $C_{15}H_{10}O_6$ | 287.0550, 258.0535, 241.0505, 213.0556, 165.0191, 153.0189 | $(M^+ H)^+$ | -1.1 |
| 17 | Isorhamnetin | 10.028 | 317.0661 | $C_{16}H_{12}O_7$ | 317.0661, 302.0428, 285.0401, 229.0500, 153.0183 | $(M^+ H)^+$ | 1.6 |
| 18 | Batatasin III | 10.437 | 245.1163 | $C_{15}H_{16}O_3$ | 245.1169, 151.0749, 137.0595, 121.0646, 107.0490, 91.0540 | $(M^+ H)^+$ | -3.8 |
| 19 | Trans-pterostilbene | 11.524 | 257.1160 | $C_{16}H_{16}O_3$ | 257.1169, 242.0931, 226.0979, 211.0748, 197.0955, 181.0643 | $(M^+ H)^+$ | -4.7 |
| 20 | Linoleic acid | 13.289 | 281.2471 | $C_{18}H_{32}O_2$ | 281.2490, 155.1437, 109.1016, 95.0858, 81.0703, 67.0545 | $(M^+ H)^+$ | -1.5 |
| 21 | E-resveratrol trimethyl ether | 14.038 | 271.1320 | $C_{17}H_{18}O_3$ | 271.0324, 255.1024, 240.1141, 225.0909, 209.0964, 165.0698 | $(M^+ H)^+$ | -3.2 |
| 22 | Oleanonic acid | 16.950 | 455.3531 | $C_{30}H_46O_3$ | 455.3499, 381.3399, 269.2257, 238.1526, 81.0695 | $(M^+ H)^+$ | 2.5 |
| 23 | 4-hydroxybenzaldehyde | 6.082 | 121.0291 | $C_7H_6O_2$ | 121.0290, 92.0263, 75.0232 | $(M^- H)^-$ | -3.3 |
| 24 | p-Coumaric acid | 6.630 | 163.0398 | $C_9H_8O_3$ | 163.0392, 119.0503, 93.0344 | $(M^- H)^-$ | -1.7 |
| 25 | Vitexin | 6.752 | 431.0987 | $C_{21}H_{20}O_{10}$ | 431.0973, 341.0667, 311.0553, 283.0606, 269.0455 | $(M^- H)^-$ | 0.8 |
| 26 | Quercetin 3-galactoside | 6.857 | 463.0870 | $C_{21}H_{20}O_{12}$ | 463.0866, 300.0261, 271.0235, 255.0283, 243.0290, 151.0033 | $(M^- H)^-$ | -2.6 |
| 27 | Kaempferol-3-O-rutinoside | 7.049 | 593.1497 | $C_{27}H_{30}O_{15}$ | 593.1489, 447.0949, 327.0507, 285.0384, 255.0284, 151.0035 | $(M^- H)^-$ | -2.5 |
| 28 | Pinoresinol | 7.208 | 357.1343 | $C_{20}H_{22}O_6$ | 357.1247, 160.0532, 151.0405, 136.0167, 122.0383, 92.0261 | $(M^- H)^-$ | -0.2 |
| 29 | Kaempferol 3-O-glucoside | 7.261 | 447.0919 | $C_{21}H_{20}O_{11}$ | 447.0923, 284.0316, 255.0285, 227.0336, 163.0612 | $(M^- H)^-$ | -3.1 |
| 30 | Kaempferol-3-O-α-L-arabinoside | 7.543 | 417.0824 | $C_{20}H_{18}O_{10}$ | 417.0818, 284.0327, 255.0300, 227.0352 | $(M^- H)^-$ | -0.8 |
| 31 | Azelaic acid | 7.723 | 187.0970 | $C_9H_{16}O_4$ | 187.0962, 169.0864, 143.1062, 125.0970, 97.0657, 57.0345 | $(M^- H)^-$ | -3.1 |

Table I. Continued.

| No. | Compound name | RT, min | Measured value, m/z | Molecular formula | MS/MS | Ion species | Error, ppm |
|---|---|---|---|---|---|---|---|
| 32 | Kaempferol-3-O-α-L-rhamnoside | 8.044 | 431.0980 | $C_{21}H_{20}O_{10}$ | 431.0978, 284.0319, 269.0460, 255.0293, 227.0342 | $(M-H)^-$ | -0.9 |
| 33 | Coelonin | 8.290 | 241.0873 | $C_{15}H_{14}O_3$ | 431.0978, 284.0319, 269.0460, 255.0293, 227.0342 | $(M-H)^-$ | 1.2 |

MEAG, methanolic extract of BaiYangJie; RT, retention time; MS/MS, tandem mass spectrometry.

total of 210 intersecting targets were obtained by intersecting the drug and disease targets (Fig. 2A).

The PPI network reflects protein interactions; 210 intersecting targets formed a network with 208 nodes and 2,861 edges. Subsequently, the PPI network was visualised using Cytoscape and the topology analysis was performed using the 'CytoNCA' plug-in. The top 15 nodes of the network were sorted by betweenness centrality, closeness centrality and degree centrality values and the hub targets were the intersection of these three values. These hub targets were AKT1, EGFR, ALB, BCL2, HIF1A, HSP90AA1, SRC, ESR1, PTGS2, MAPK3 and GSK3B (Fig. 2B and C; Table SII).

Based on GO functional enrichment, biological process enrichment involved 'cellular response to lipid' and 'cellular response to chemical stress', 'regulation of inflammatory response' and 'positive regulation of programmed cell death'. Cellular component enrichment included 'perinuclear region of cytoplasm', 'centrosome' and 'basal plasma membrane'. Molecular function enrichment involved 'protein kinase activity' and 'protein tyrosine kinase activity' (Fig. 2D). Collectively, MEAG may have contributed to the treatment of Cis-AKI through the regulation of numerous components, targets and pathways.

The target set was imported into the Metascape database for KEGG pathway and biological process enrichment analysis. There were 184 KEGG pathways associated with Cis-AKI therapy in mice. In addition to the cancer pathway with the largest number of annotation genes, the target set was also closely associated with 'FoxO signalling pathway', arachidonic acid metabolism', 'NF-κB signalling pathway' and 'TGF-β signalling pathway' (Fig. 2E).

*Serum metabolomics*

*Multivariate statistical analyses*. General distribution of samples was examined by PCA, with results showing the QC samples clustered together, indicating that the instrument was stable (Fig. 3A and B). The three groups of test samples were clustered, which indicated similarities within the data. There were notable metabolic differences among the three groups. The Nor group was clearly separated from the Cis group and the MEAG group exhibited a downward trend after treatment, indicating that MEAG exerted an ameliorative effect on metabolic disorders in Cis-AKI model mice (Fig. 3A and B).

To establish an association model between the expression of metabolites and sample categories and to screen the differential metabolites, OPLS-DA in positive and negative ion mode was used (Fig. 3C, E, G and I) and the samples in the Nor and Cis groups and Cis and MEAG groups were all significantly separated.

The S-plot diagram of positive and negative ions showed differences in metabolites between the Nor and Cis groups and between the Cis and MEAG groups (Fig. 3D, F, H and J). VIP, fold change (FC) and P-values were then used to identify characteristic differentially expressed metabolites among the three groups. Thus, substances with $\log_2$ (FC) >1, VIP >1 and P<0.05 were potentially upregulated differential metabolites and substances with $\log_2$ (FC)<-1, VIP>1 and P<0.05 were potential downregulated differential metabolites. In the positive ion

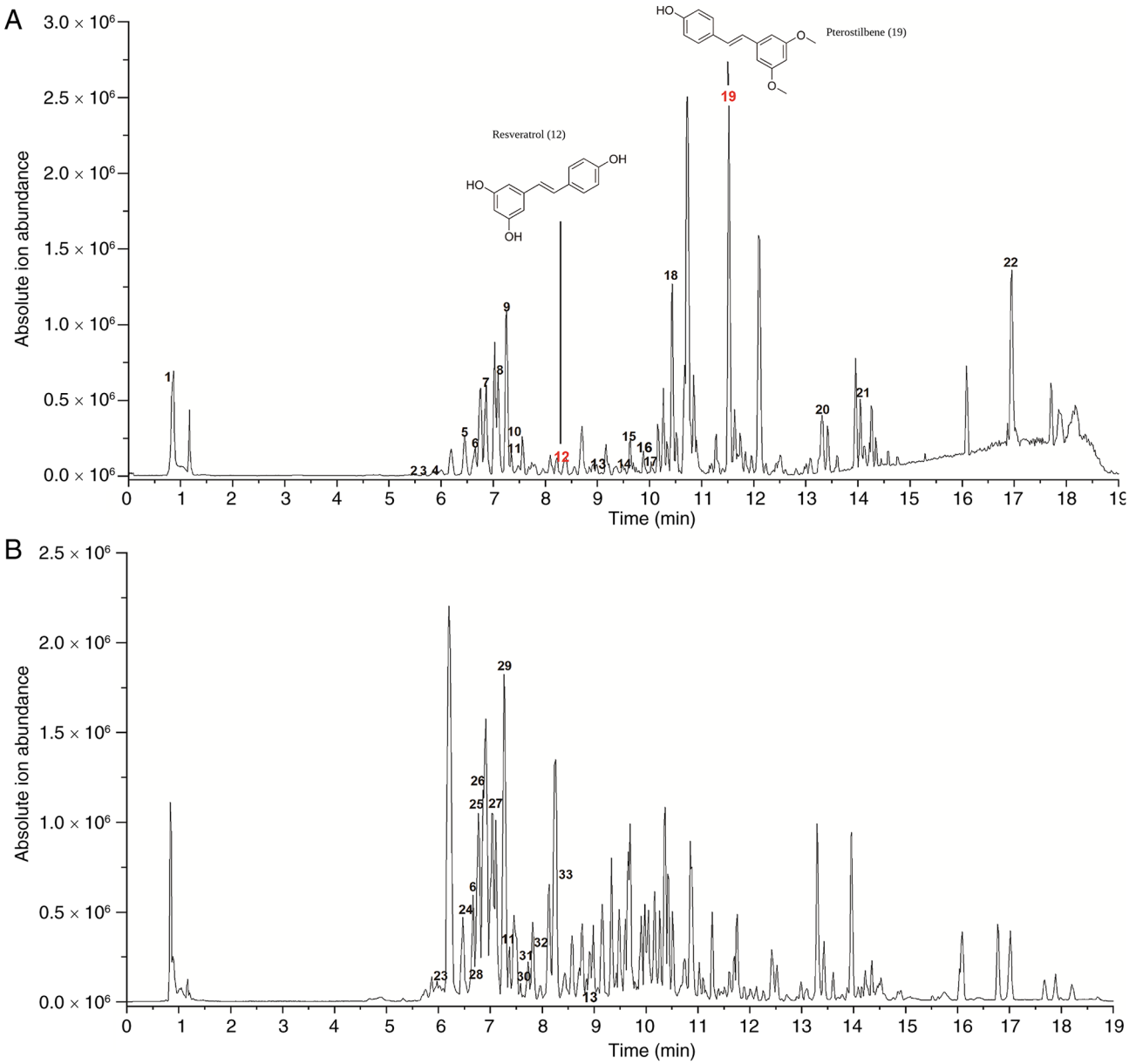


Figure 1. Base peak chromatogram of methanolic extract of BaiYangJie. (A) Positive ion modes and (B) negative ion modes.

mode, six endogenous differential metabolites were identified between Nor and Cis groups, and Cis and MEAG groups, including L-phenylalanine, L-carnitine, creatine, phosphocholine, lysophosphatidylethanolamine (LysoPE 16:0/0:0, the notation 16:0/0:0 indicates the fatty acyl chain composition, with a 16-carbon saturated fatty acyl chain and no second fatty acyl chain) and stearoyl-L-carnitine. In negative ion mode, eight endogenous differential metabolites were identified between the Nor and Cis groups and the Cis and MEAG groups, including L-tryptophan, citric acid, ascorbic acid, L-phenylalanine, hyocholic acid, docosahexaenoic acid, L-tyrosine and L-pyroglutamic acid. All differential metabolites in different groups were visualised as a heatmap, in which blue to red indicated an increase in the abundance of differential metabolites (Fig. 4). Table SII and Fig. 5 provide detailed information regarding each differential metabolite and the changes in the relative contents of potentially different metabolites.

*Construction and analysis of metabolic module*. Metabolite and gene regulatory network is shown in Fig. 6A. Through topological analysis of metabolic modules, phenylalanine was identified as the hub with the highest centrality. Then, MetaboAnalyst was used to analyse the metabolic pathway enrichment of the 12 metabolites. As shown in Fig. 6B, 14 pathways affecting the metabolism of mice with Cis-AKI were obtained from 13 different metabolites. Among them, the potential metabolic pathways with path influence >0.1 were 'phenylalanine metabolism' and 'phenylalanine, tyrosine and tryptophan biosynthesis'. Based on the results of metabolite network and pathway analyses, phenylalanine metabolism may be a key metabolic pathway regulated by MEAG in the treatment of Cis-AKI.

*Comprehensive analysis of network pharmacology and serum metabolomics*. Associations between metabolic pathways and their targets were next assessed. To comprehensively explore the mechanism of action of MEAG in treating Cis

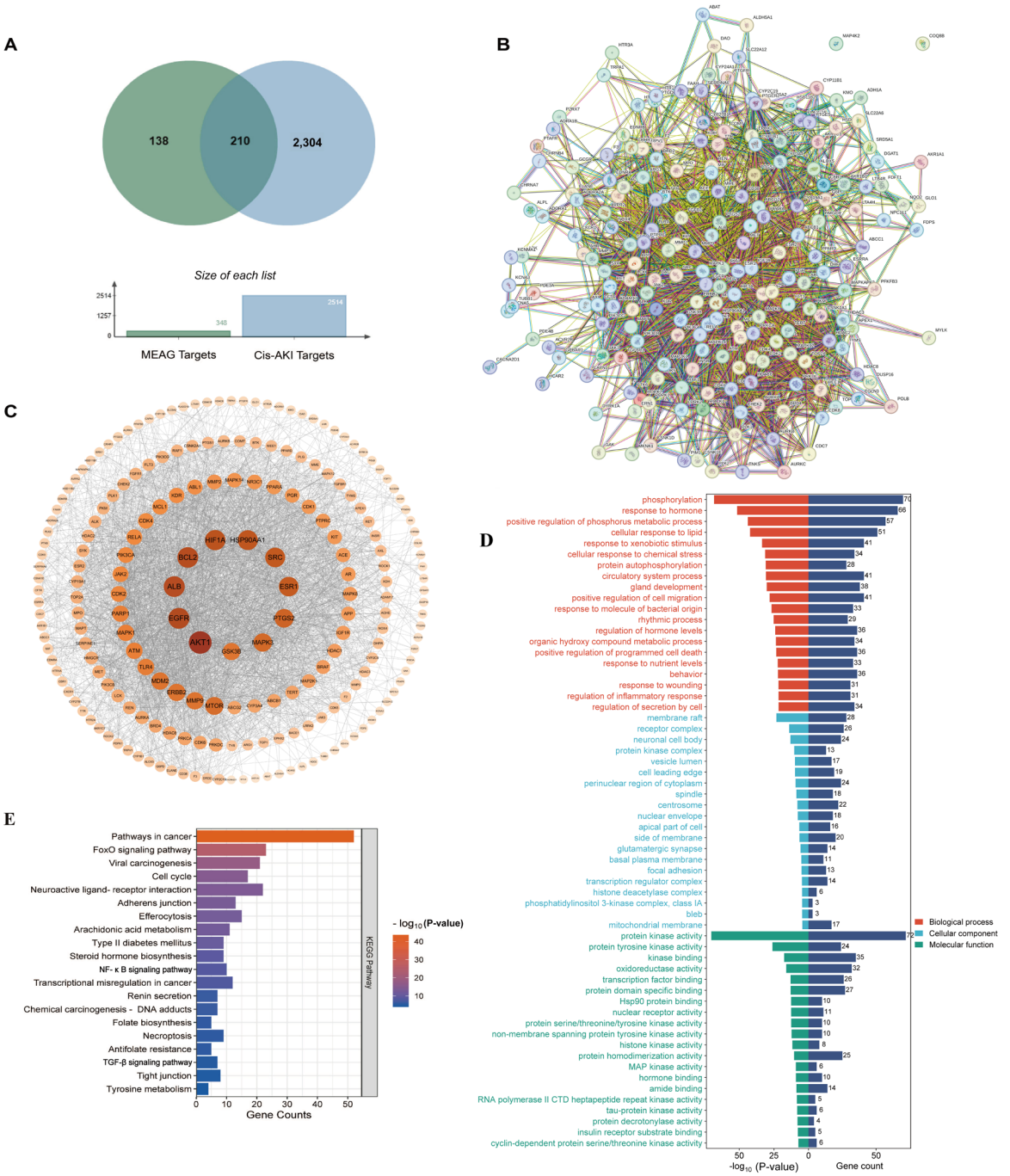


Figure 2. Therapeutic mechanisms of MEAG against Cis-AKI in murine models using network pharmacology approaches. (A) Venn analysis of common targets of MEAG-Cis-AKI in mice. (B) Protein-protein interaction network of shared MEAG and Cis-AKI targets. (C) Core protein-protein interaction network for MEAG against Cis-AKI injury. (D) Bar diagram of top 20 biological process, cellular component and molecular function terms. (E) Enrichment profile of the 20 most significant Kyoto Encyclopaedia of Genes and Genomes signalling pathways. MEAG, methanolic extract of BaiYangJie; Cis, cisplatin; AKI, acute kidney injury.

nephrotoxicity, the targets of phenylalanine metabolism were assessed using KEGG (25) and intersected with drug targets and disease targets, integrated the results of serum metabolomics and network pharmacology analysis and subsequently identified an intersection target (MIF).

Among the aforementioned key signalling pathways, NF-κB serves a central role in cellular inflammatory and immune responses (26). A previous study suggested that, in a Cis-AKI mouse model, injured renal tubular epithelial cells released inflammatory cytokines, activated the MIF/NF-κB pathway and triggered a cascade of inflammatory responses, thereby exacerbating renal tubular injury (27). In addition, phenylalanine metabolism is also associated with inflammation. Therefore, the ability of MEAG to regulate the MIF/NF-κB signalling pathway and associated inflammatory factors was evaluated. A schematic diagram of the regulatory pathway is shown in Fig. 7.

*MEAG ameliorates Cis-AKI in mice*. After intraperitoneal injection of Cis, mice exhibited clear nephrotoxicity, including

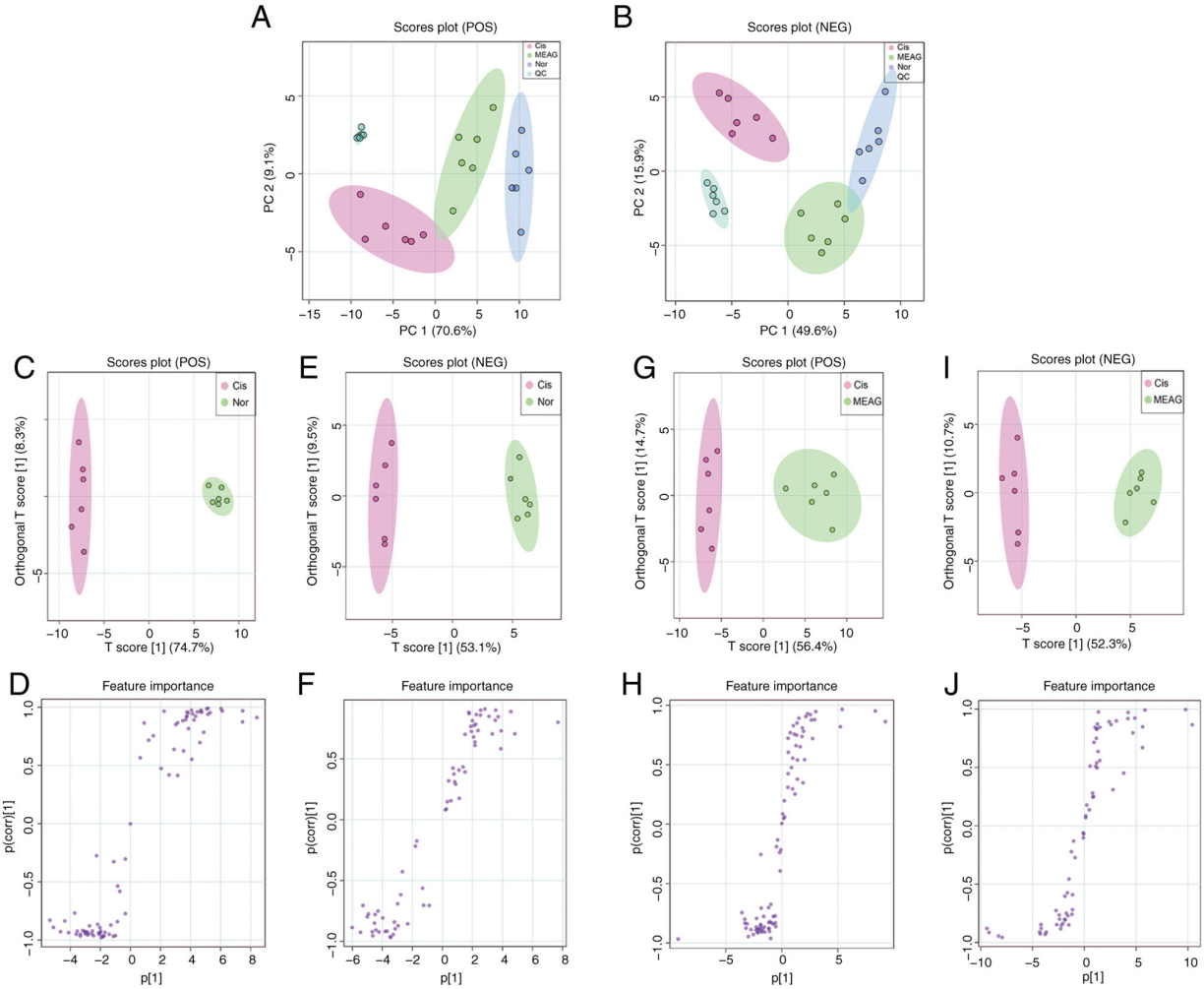


Figure 3. Multivariate statistical analyses of metabolomics in mice serum. (A) PCA score plot of serum metabolism in POS ionization mode. (B) PCA score plot of serum metabolism in NEG ionization mode. (C) OPLS-DA score plot comparing the Nor and Cis groups in POS ionization mode. (D) S-plot comparing the Nor and Cis groups in POS ionization mode. (E) OPLS-DA score plot comparing the Nor and Cis groups in NEG ionization mode. (F) S-plot comparing the Nor and Cis groups in NEG ionization mode. (G) OPLS-DA score plot comparing the Cis and MEAG groups in POS ionization mode. (H) S-plot comparing the Cis and MEAG groups in POS ionization mode. (I) OPLS-DA score plot comparing the Cis and MEAG groups in NEG ionization mode. (J) S-plot comparing the Cis and MEAG groups in NEG ionization mode. OPLS-DA, orthogonal partial least squares discriminant analysis; Nor, normal control group; Cis, cisplatin; MEAG, methanolic extract of BaiYangJie; QC, quality control; POS, positive; NEG, negative; PCA, principal component analysis.

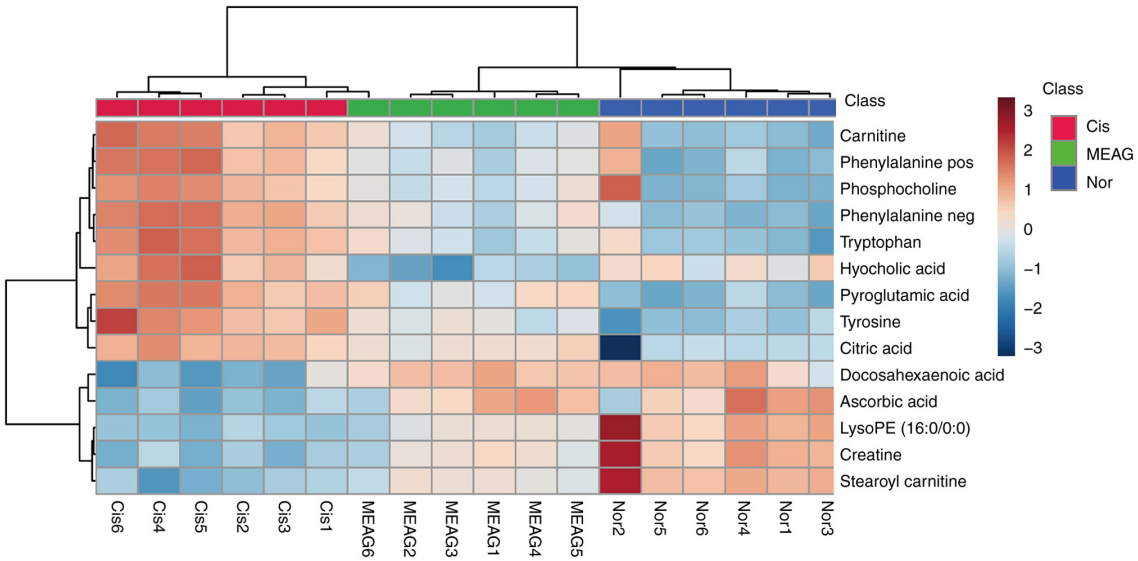


Figure 4. Cluster thermogram of all endogenous differential metabolites. Nor, normal control group; Cis, cisplatin; MEAG, methanolic extract of BaiYangJie; LysoPE, lysophosphatidylethanolamine.

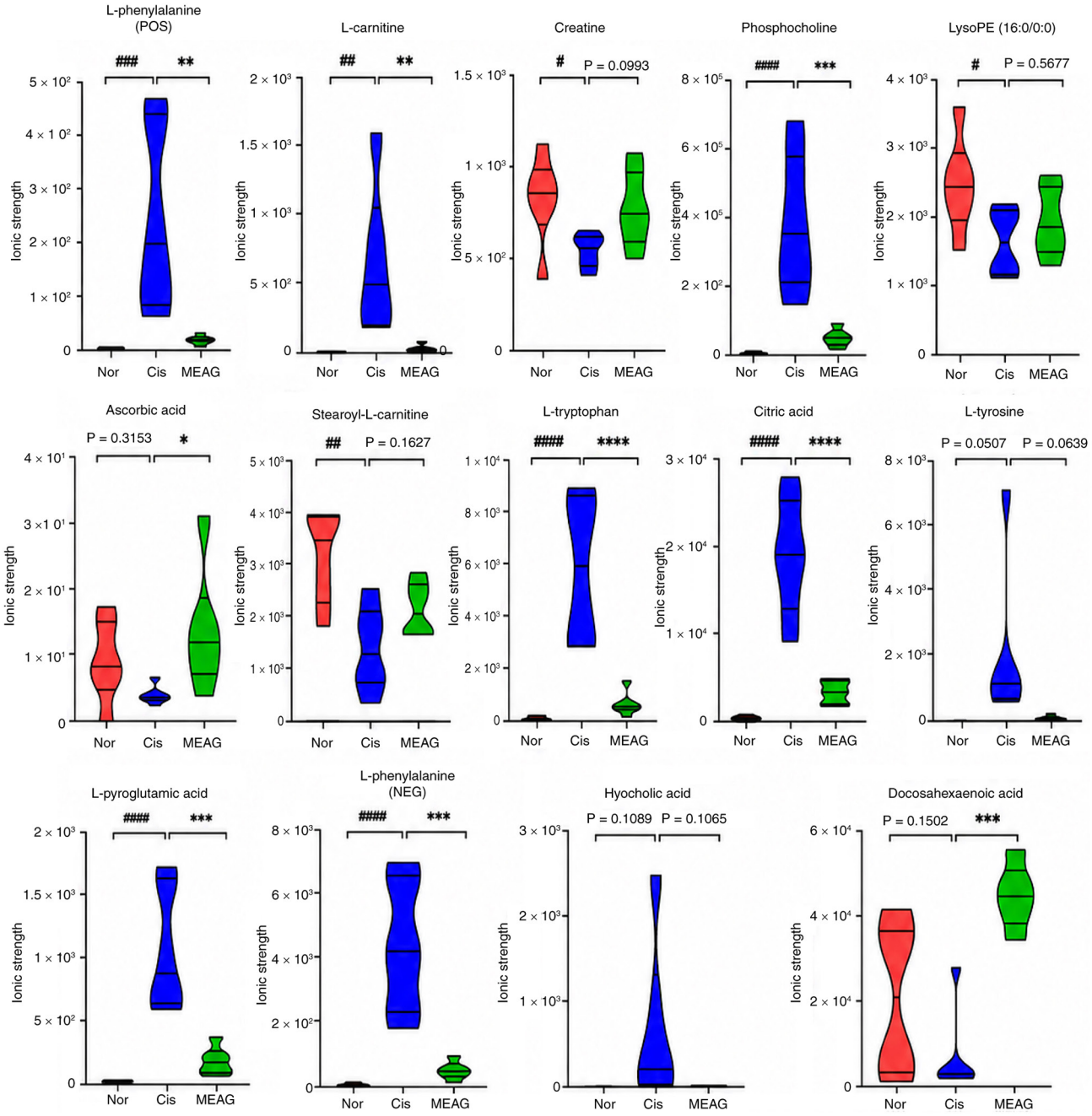


Figure 5. Relative content changes of potential metabolites. ####P<0.0001, ##P<0.01, #P<0.05; compared with the Nor group, ****P<0.0001, ***P<0.001, **P<0.01 and *P<0.05 compared with the Cis group. LysoPE, lysophosphatidylethanolamine; POS, positive; NEG, negative; Cis, cisplatin; MEAG, methanolic extract of BaiYangJie; Nor, normal control group.

weight loss and a significantly increased renal index (P<0.0001; Fig. 8A and B). The levels of Scr (P<0.0001) and BUN (P<0.0001) also increased significantly (Fig. 8C and D). H&E staining of renal tissue showed that intraperitoneal injection of Cis caused serious damage to renal tubules and glomeruli, with renal tubular dilatation, renal tubular epithelial cell shedding, gelatinous casts, glomerular atrophy and basement membrane thickening (Fig. 8E). Quantitative analysis further showed that the tubular injury score was significantly increased in the Cis group compared with that in the Nor group (P<0.0001; Fig. 8F). Masson's trichrome staining revealed severe fibrosis in renal tissue (Fig. 8G). Consistently, the collagen volume fraction was significantly increased in the Cis group compared with that in the Nor group (P<0.0001; Fig. 8H). MEAG treatment significantly ameliorated the loss of renal function of mice and significantly reduced the kidney index (P<0.001; Fig. 8B) and levels of Scr (P<0.0001) and BUN (P<0.0001), which were increased by Cis injection (Fig. 8C and D). Simultaneously, MEAG ameliorated renal tubular damage and reduced the degree of renal tissue fibrosis (Fig. 8E-H).

KIM-1 and NGAL are biomarkers of AKI (28). The expression and distribution of KIM-1 and NGAL in renal tissue were examined. IHC staining showed that the expression of KIM-1 (P<0.0001) and NGAL (P<0.0001) in mouse renal tissue significantly increased after Cis injection and were significantly reduced by MEAG treatment (P<0.0001; Fig. 9A-D).

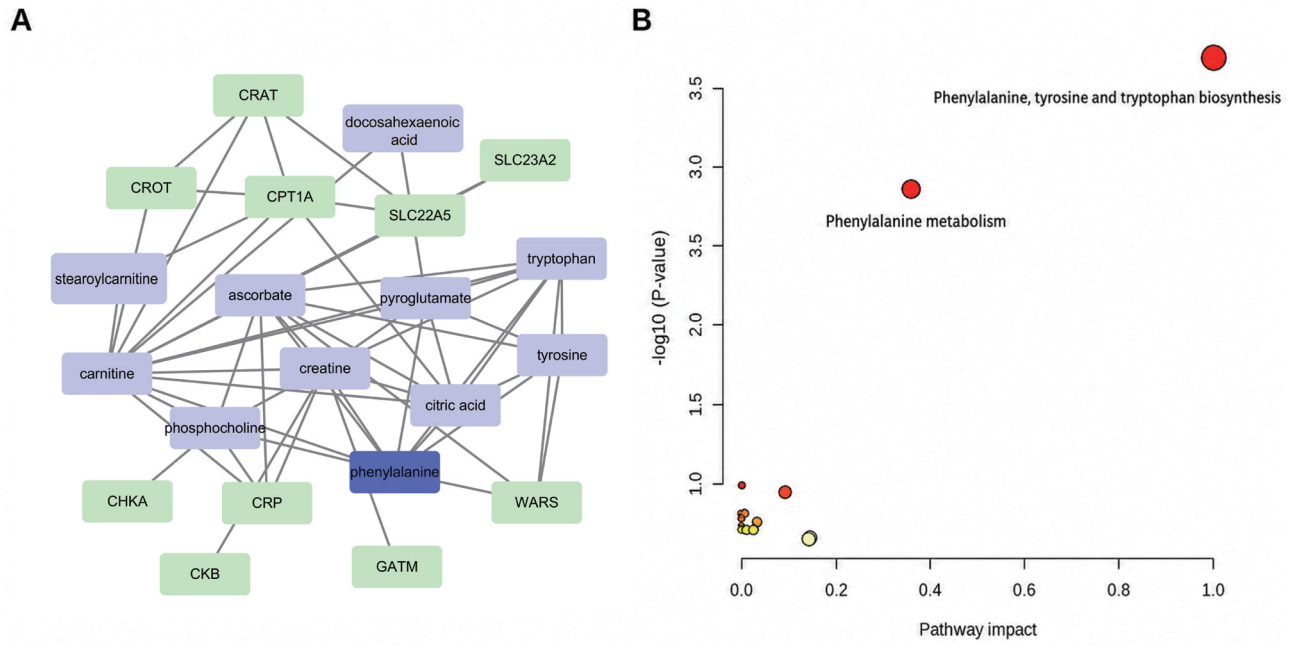


Figure 6. Metabolic pathway analysis. (A) Metabolic modules regulated by the methanolic extract of BaiYangJie. (B) Association diagram of 'phenylalanine metabolism' and 'phenylalanine, tyrosine and tryptophan biosynthesis'.

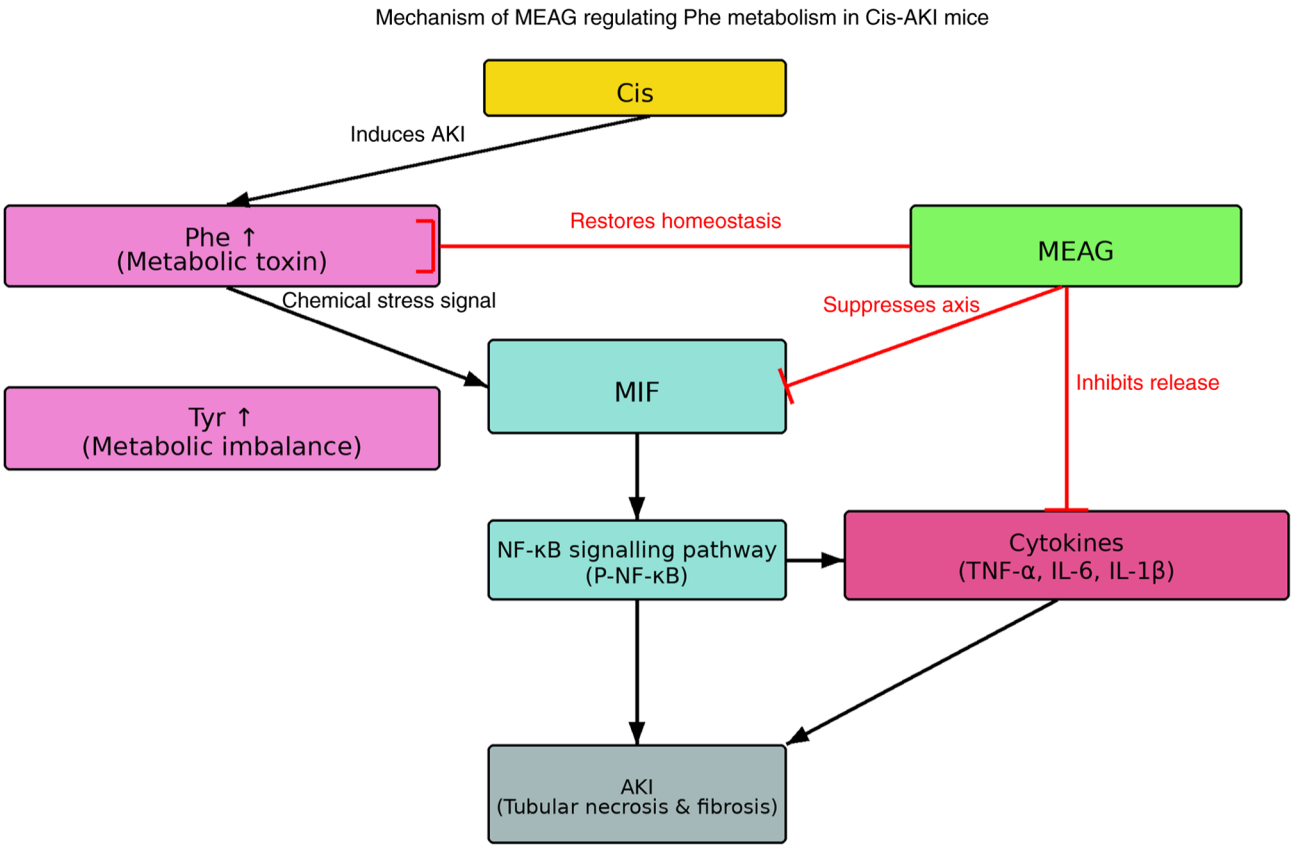


Figure 7. Schematic diagram of MEAG regulating phenylalanine metabolic flux. MEAG, methanolic extract of BaiYangJie; Cis, cisplatin; Cis-AKI, cisplatin-induced acute kidney injury; Phe, phenylalanine; Tyr, tyrosine; MIF, macrophage migration inhibitory factor; NF-κB, nuclear factor κB; P-NF-κB, phosphorylated NF-κB; TNF-α, tumor necrosis factor α; IL-6, interleukin-6; IL-1β, interleukin-1β; AKI, acute kidney injury.

*MEAG ameliorates inflammatory responses in mice treated with Cis*. Proinflammatory cytokine expression in mice after MEAG treatment was analysed. ELISA data showed that MEAG significantly reduced the increase in IL-1β ($P<0.0001$), IL-6 ($P<0.0001$) and TNFα ($P<0.0001$) levels in the serum of mice initially induced by Cis (Fig. 10A-C). Furthermore,

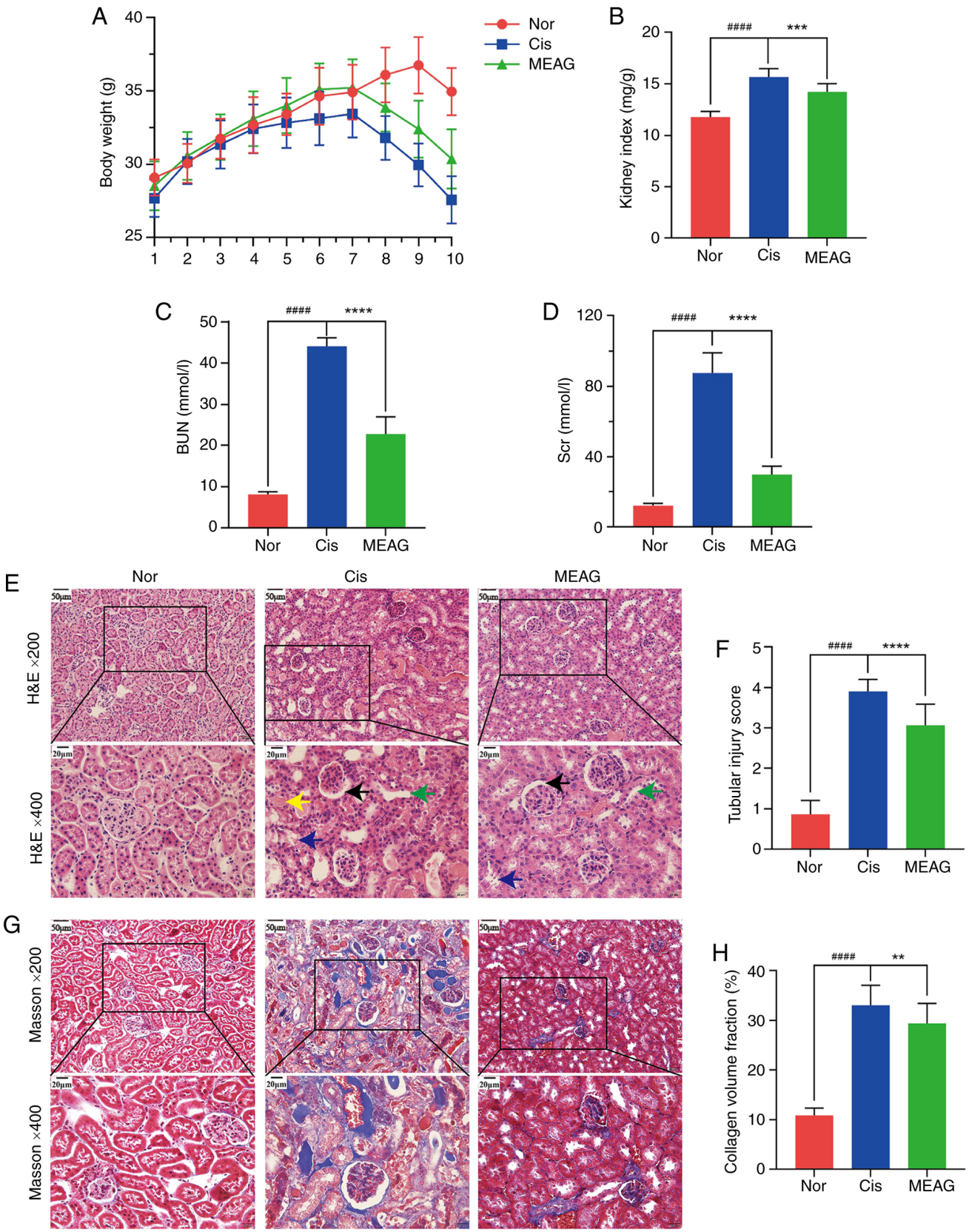


Figure 8. MEAG treatment ameliorated Cis-AKI in mice. (A) Effect of MEAG on body weight change in mice with Cis-AKI. (B) Effect of MEAG on kidney index in mice with Cis-AKI. (C) Effect of MEAG on BUN levels in mice with Cis-AKI. (D) Effect of MEAG on Scr levels in mice with Cis-AKI. (E) Representative H&E-stained kidney sections from the Nor, Cis, and MEAG groups, shown at x200 magnification with corresponding higher-magnification views at x400. Yellow arrows indicate rubber-like tubular casts, blue arrows indicate shedding of renal tubular epithelial cells, green arrows indicate renal tubular dilatation, and black arrows indicate glomerular atrophy and basement membrane thickening. (F) Tubular injury score in each group. (G) Representative Masson-stained kidney sections from the Nor, Cis and MEAG groups, shown at x200 magnification with corresponding higher-magnification views at x400. (H) Collagen volume fraction in each group. Data in panels (A-D), (F) and (H) are presented as mean ± SD (n=6 mice per group). $^{\#\#\#\#}$P<0.0001 compared with the Nor group; $^{**}$P<0.01, $^{***}$P<0.001 and $^{****}$P<0.0001 compared with the Cis group. Scale bars, 50 $\mu$m for x200 images and 20 $\mu$m for x400 images. Nor, normal control group; Cis, cisplatin; MEAG, methanolic extract of BaiYangJie; AKI, acute kidney injury; Scr, serum creatinine; BUN, blood urea nitrogen.

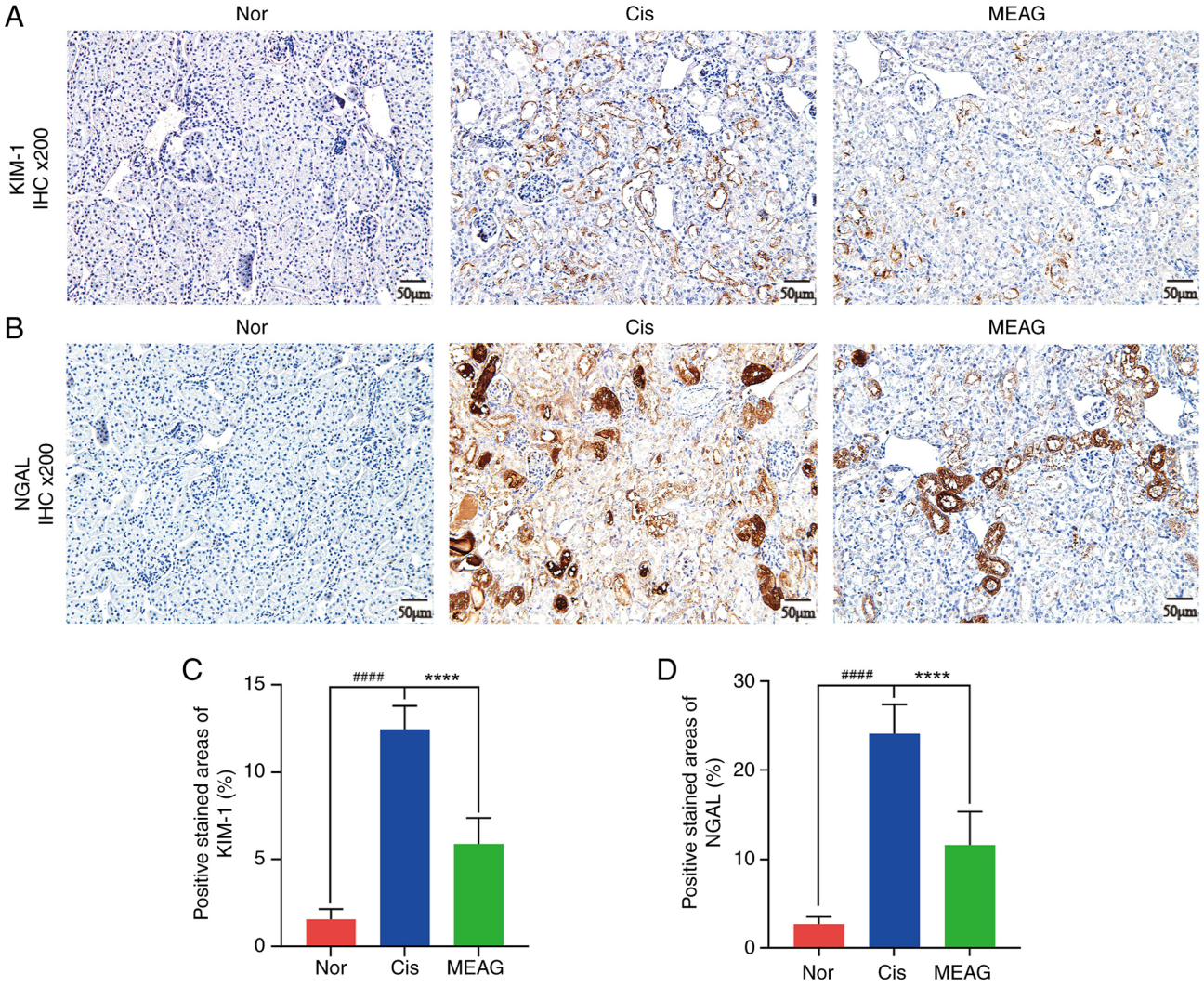


Figure 9. Upregulation of KIM-1 and NGAL expression induced by cisplatin was reduced by MEAG. (A) Representative IHC images of KIM-1 expression in kidney tissues from the Nor, Cis and MEAG groups. (B) Representative IHC images of NGAL expression in kidney tissues from the Nor, Cis and MEAG groups. (C) Quantitative analysis of the positive stained area of KIM-1 in kidney tissues. (D) Quantitative analysis of the positive stained area of NGAL in kidney tissues. For panels (A) and (B), magnification x200 and scale bar, 50 $\mu$m. For panels (C) and (D), data are presented as mean ± SD (n=3 per group). $^{####}$P<0.0001, compared with the Nor group and $^{****}$P<0.0001, compared with the Cis group. Nor, normal control group; Cis, cisplatin; MEAG, methanolic extract of BaiYangJie; IHC, immunohistochemistry; NGAL, neutrophil gelatinase-associated lipocalin; KIM-1, kidney injury molecule 1.

western blotting showed that Cis significantly induced the expression of the inflammatory factors Il-1β (P<0.0001), IL-6 (P<0.0001) and TNF-α (P<0.0001) and that this induction was attenuated by MEAG treatment (Fig. 10F and H-J). These findings indicated that MEAG reduced the inflammatory response of mice following Cis treatment.

*MEAG alleviates Cis-AKI in mice by regulating MIF/NF-κB expression*. MIF expression profiles were quantitatively assessed by IHC and western blotting. Histopathological examination demonstrated a significant elevation of MIF immunoreactivity in Cis-challenged murine models compared with the Nor group (P<0.0001), which was attenuated following MEAG intervention (P<0.0001; Fig. 10D and E). Western blotting quantification further demonstrated a significant reduction in renal MIF protein content following MEAG intervention compared with the Cis group (P<0.01; Fig. 10F and G), corroborating the histopathological observations. In addition, a comparative analysis between experimental groups revealed significantly enhanced p-NF-κB/NF-κB levels in the Cis-treated group in comparison with the Nor group (P<0.001), whereas MEAG administration significantly suppressed this phosphorylation event (P<0.01; Fig. 10K and L). These collective findings demonstrate that MEAG treatment exerts regulatory effects on the pathological activation of the MIF/NF-κB signalling cascade in Cis-induced AKI models.

## Discussion

Cis-induced nephrotoxicity manifests through a number of pathological mechanisms, with acute tubular necrosis and acute inflammatory responses being the most prevalent and notable (29,30). As Cis is primarily excreted through the kidneys, it is dependent on glomerular filtration and secretion through the proximal renal tubules (31). Cis accumulates in the proximal renal tubule fluid and spreads to high-permeability renal tubular epithelial cells (19). After renal tubular epithelial cells ingest Cis, a large number of cells are damaged, eventually

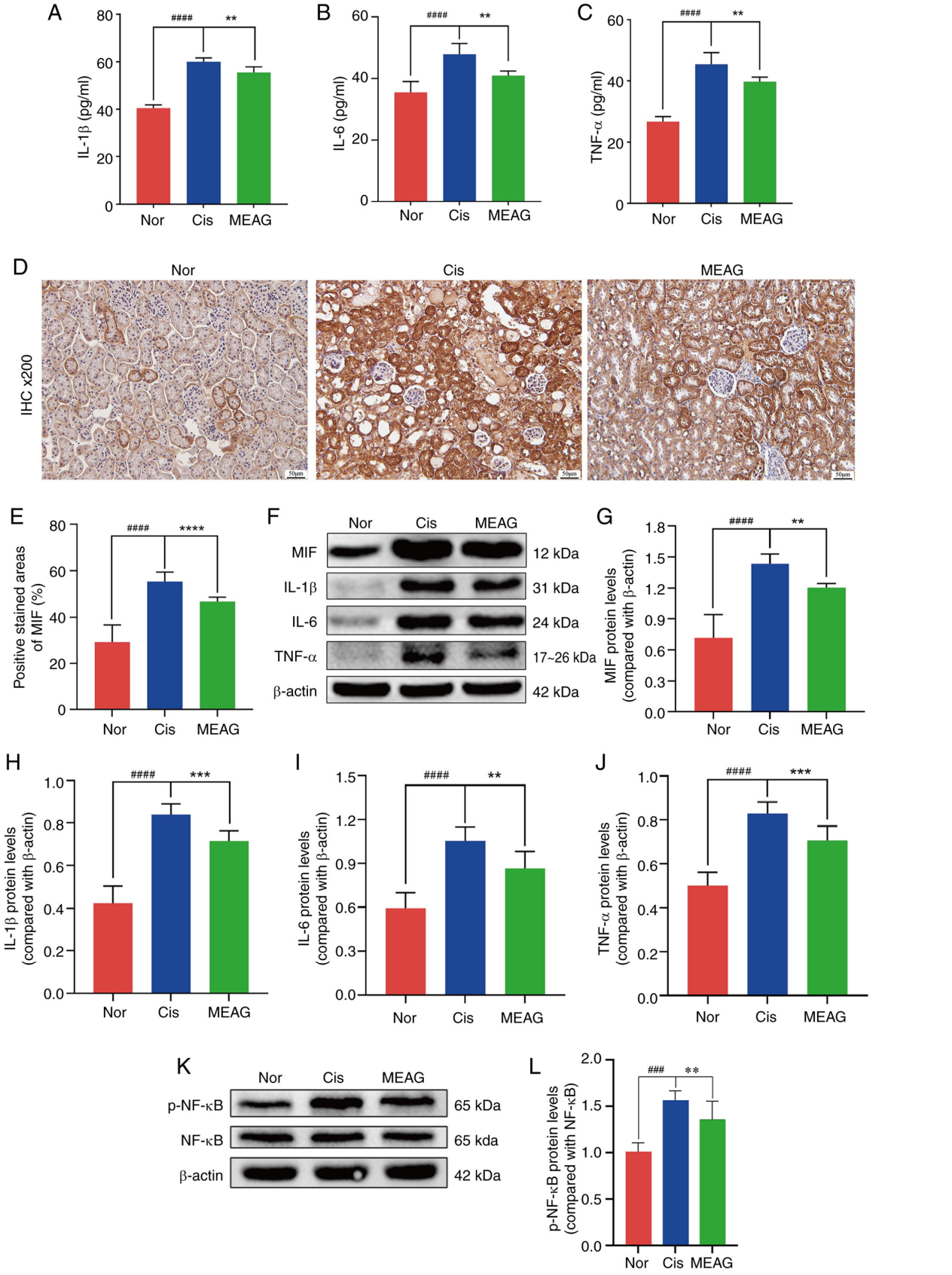


Figure 10. MEAG alleviated Cis-AKI in mice by regulating the expression of MIF/NF-κB. (A-C) Serum concentrations of pro-inflammatory cytokines (A) IL-1β, (B) IL-6 and (C) TNF-α were quantified through ELISA across experimental cohorts (n=3/group). (D) Renal tissue MIF distribution patterns visualized through IHC staining (n=3/group). (E) Semiquantitative evaluation of MIF immunoreactivity intensity. (F) Western blotting profiles demonstrating protein expression alterations in MIF, p-NF-κB, IL-1β, IL-6 and TNF-α protein levels. (G-J) Densitometric analysis of (G) MIF, (H) IL-1β, (I) IL-6 and (J) TNF-α (n=3/group). (K) Western blotting profiles demonstrating protein expression alterations in p-NF-κB and NF-κB. (L) Densitometric analysis of p-NF-κB/NF-κB (n=3/group). $^{\#\#\#\#}$P<0.0001, $^{\#\#\#}$P<0.001, compared with the Nor group; $^{****}$P<0.0001, $^{***}$P<0.001 and $^{**}$P<0.01, compared with the Cis group. Magnification, x200 and scale bar, 50 $\mu$m. Nor, normal control group; Cis, cisplatin; MEAG, methanolic extract of BaiYangJie; AKI, acute kidney injury; IHC, immunohistochemistry; MIF, migration inhibitory factor; p-, phosphorylated.

leading to acute renal tubular necrosis. In the present study, the histological examination revealed evidence of renal tubular necrosis following MEAG treatment and the results showed that MEAG significantly ameliorated Cis-induced renal tubular epithelial cell injury and necrosis.

Renal tubular epithelial cells secrete a number of inflammatory cytokines and chemokines that induce inflammation following damage (32). Among these inflammatory factors, TNF-α is an important regulatory component (33). Following Cis-induced nephrotoxicity in mice, large quantities of TNF-α may be produced. By inducing the expression of endothelial adhesion molecules and chemokines, inflammatory leukocytes migrate to the site of renal injury and stimulate the production of additional inflammatory cytokines and chemokines, including IL-6 and IL-1β, thereby promoting the local accumulation of immune effector cells and further amplifying TNF-α-mediated inflammation (34). Consistent with previous studies, the present study showed that Cis injection induced a severe inflammatory reaction and significantly increased the expression of pro-inflammatory cytokines (35,36).

To more comprehensively investigate the physiological changes associated with AKI, metabolomics was used to characterise metabolic network changes during AKI and to analyse differential metabolites in the treatment of Cis-AKI. The results showed that the phenylalanine metabolic pathway was the most notable. Phenylalanine is a key amino acid, with previous studies having shown that phenylalanine levels increase in patients with AKI (37-39). When phenylalanine levels are high, it acts as a metabolic toxin, resulting in adverse health effects, which are common in chronic inflammation and septic shock (40,41). Phenylalanine hydroxylase converts L-phenylalanine into L-tyrosine (42) and L-tyrosine accumulation may lead to changes in energy metabolism, inflammation and systemic immunity (43). The results of the present study showed that Cis disrupted amino acid metabolism in normal kidney tissue, leading to increased levels of phenylalanine and tyrosine and resulting in inflammatory reactions in the kidney. The metabolic levels of phenylalanine and tyrosine were reduced following MEAG treatment, demonstrating that MEAG effectively ameliorated the inflammatory response.

A total of 13 endogenous metabolites were identified as differentially expressed in the present study. In addition to phenylalanine, the other metabolites were primarily involved in amino acids, lipid and energy metabolisms and the antioxidant system, all of which are closely associated with the pathophysiological processes and inflammatory responses associated with Cis-AKI. Among amino acid metabolites, L-tryptophan is a precursor in tryptophan metabolism and its metabolic disorder leads to an imbalance in the kynurenine pathway, thereby exacerbating oxidative stress and inflammatory responses in renal tissue (44). L-pyroglutamic acid is a key intermediate of glutamine metabolism, and Cis-induced deviations in its level from that of the Nor group are associated with energy metabolism disorders and renal tubular epithelial apoptosis in renal injury (45). MEAG reversed these Cis-induced abnormal changes in L-tryptophan and L-pyroglutamic acid levels, alleviating the overall imbalance in the amino acid metabolic network. Among lipid metabolism-related substances, L-carnitine and stearoyl-L-carnitine were involved in the β-oxidation of fatty acids, their Cis-induced deviations from the Nor group levels reflected mitochondrial lipid metabolism disorders in the kidney during Cis-AKI. Impaired mitochondrial function can further trigger oxidative stress and the release of inflammatory factors (46).

LysoPE (16:0/0:0) and docosahexaenoic acid (DHA) are important components of phospholipid metabolism. Compared with the Nor group, LysoPE (16:0/0:0) was increased in the Cis group, which may impair the integrity of renal tubular cell membranes, whereas DHA was decreased in the Cis group, weakens its anti-inflammatory and antioxidant effects (47). The regulation of the aforementioned lipid metabolites by MEAG restored the physiological state of renal lipid metabolism and alleviated cell membrane damage and inflammatory responses. Among energy metabolism-associated substances, citric acid is a core intermediate of the tricarboxylic acid cycle and creatine and phosphocholine are involved in cellular energy storage and transport; Cis-induced deviations in the levels of citric acid, creatine and phosphocholine from those of the Nor group indicated disruption of tricarboxylic acid cycle activity and cellular energy storage and transport, and renal tubular epithelial cells undergo injury and necrosis due to energy deficiency (48). However, MEAG restored these metabolites to normal levels, improved energy metabolism in renal tissue and provided energy support for cell repair. The levels of the antioxidant ascorbic acid (vitamin C) were decreased in Cis-AKI, reflecting high consumption by the renal antioxidant system and thus, a cycle between oxidative stress and inflammatory responses was formed (49,50). Furthermore, MEAG upregulated vitamin C levels, enhanced the antioxidant capacity of the kidney, reduced reactive oxygen species production and thereby inhibited the release of inflammatory factors. The aforementioned differential metabolites jointly constitute a network of renal metabolic disorders in Cis-AKI. MEAG can regulate key nodes of this network through numerous targets, thereby synergistically restoring metabolic homeostasis and alleviating renal injury and inflammatory responses. This regulatory effect synergises with the regulation of phenylalanine metabolism and together mediates the protective effect of MEAG on Cis-AKI.

A total of 210 potential MEAG targets against Cis-AKI were identified across all disease databases and potential drug targets. By analysing the DC, BC and CC values of the PPI network, 11 core targets were identified, including AKT1, EGFR, ALB, BCL2, HIF1A, HSP90AA1, SRC, ESR1, PTGS2, MAPK3 and GSK3B, which may serve key roles in the MEAG interaction network targeting Cis-AKI. Inhibiting AKT1 expression reduces oxidative stress in cells and the levels of inflammatory factors such as IL-1β and IL-6 (51). MAPK3 is the final component of the MAPK phosphorylation cascade and an important member of the MAPK signalling pathway (52), where it serves central roles in responses to numerous forms of stress and injury, such as oxidative stress, inflammatory stimulation and metabolic stress, as well as in the pathophysiology of a number of diseases, including renal tubular inflammation and diabetic nephropathy (53). SRC family kinases are non-receptor tyrosine kinases and their abnormalities can lead to inflammation, autoimmune diseases and cancer, including colorectal, breast and lung cancer (54).

Macrophage MIF is a pro-inflammatory cytokine and an important upstream mediator of innate immunity, adaptive

immunity and survival pathways, including MAPK/ERK and PI3K/AKT signalling pathways (55), which can activate macrophages and T lymphocytes, regulating pathological processes, including leukocyte recruitment, inflammation, immune responses, cell proliferation, tumourigenesis and the reverse regulation of glucocorticoids (56). Under physiological circumstances, the expression of MIF in renal tissue is low (57). However, following AKI, severe renal inflammation occurs, including macrophage and T cell infiltration. Thus, the expression of MIF is markedly increased (58). In the present study, it was determined that MIF expression in the renal tissue of mice in the Cis group was significantly increased and associated with the severity of renal tubular necrosis. MIF is associated with the NF-κB pathway. Once released, MIF binds CD74 to initiate the membrane recruitment of CD44, resulting in the activation of the NF-κB signalling pathway, the expression of TNF-α, IL-1β and IL-6 increases and macrophages, neutrophils and T cells are recruited and activated, exacerbating AKI (59).

The results of the present study showed that MEAG significantly reduced the expression levels of MIF and the NF-κB signalling pathway and reduced MIF-mediated TNF-α, IL-6 and IL-1β levels, effectively inhibiting the inflammatory reaction and improving Cis-AKI. In particular, NF-κB does not exist as an independent signal pathway and it may directly or indirectly regulate other molecules in addition to MIF, including previously reported (60). A previous study showed that NF-κB inhibited TNF-induced apoptosis of rat hepatocytes by downregulating JNK and c-Jun/activator protein-1 (61). There appears to be an association between STAT3 and NF-κB. IL-6 is a gene product regulated by the NF-κB signal and an important STAT3 activator (62). In renal diseases, NF-κB not only participates in the transcription of pro-inflammatory genes in T helper (Th)-1 and Th17 cells, but also promotes their differentiation into CD4 T cells through interaction with innate immune cells (63). In addition, mesangial epithelial cells and renal tubular epithelial cells can also promote inflammation through toll-like receptor/NF-κB axes (64). The discovery of these synergistic regulatory effects may highlight a novel direction for further exploring the mechanism of MEAG in treating Cis-AKI.

Notably, integrated analysis suggested that MIF served as a pivotal molecular bridge associating phenylalanine metabolic dysfunction with NF-κB-mediated inflammatory responses. In the context of Cis-AKI, renal dysfunction leads to the marked accumulation of phenylalanine and its downstream metabolite, tyrosine (65). These metabolites act as 'metabolic toxins' that can directly trigger or exacerbate chemical stress and inflammatory reactions within the renal microenvironment (66). Database intersection analysis identified MIF as a key target within the phenylalanine metabolic pathway. Thus, it was hypothesised that stress signals arising from metabolic imbalances (specifically, accumulation of phenylalanine) may upregulate MIF expression. Once upregulated, MIF binds to its receptor complex, activating NF-κB-mediated signalling cascade and leading to the release of pro-inflammatory cytokines such as TNF-α, IL-6 and IL-1β, thereby forming a cycle between metabolic disorder and inflammatory injury. The therapeutic efficacy of MEAG is characterised by a 'dual-regulatory' strategy; it not only restores phenylalanine metabolic homeostasis, thereby reducing the production of metabolic toxins, but also directly suppresses the pathological activation of the MIF/NF-κB axis. This synergistic modulation of metabolic and immune pathways provides a systematic pharmacological basis for the renoprotective effects of MEAG against chemotherapy-induced nephrotoxicity.

Collectively, the results of the present study showed that MEAG may serve a role in the treatment of Cis-AKI by regulating numerous targets and signalling pathways. However, there were also a number of limitations, such as the lack of a positive drug control group, incomplete data searches, insufficient coverage of Traditional Chinese Medicine components and dependence on calculation and prediction. A positive control group was not established in the present study, as to the best of our knowledge, there are currently no specific drugs for Cis-AKI in clinical practice. Furthermore, network pharmacology analysis in the present study failed to clearly illustrate the direct binding association between specific chemical components in MEAG and the targets associated with the MIF/NF-κB signalling pathway or phenylalanine metabolism. The potential bioactive components and core targets were only screened through component-target-pathway analysis, without conducting molecular docking simulation or *in vitro* binding verification, meaning it was not possible to clarify the direct interaction mode and binding affinity between single components or component combinations and core targets and also hindered the accurate interpretation of the structure-activity association between the material basis of the renoprotective effect of MEAG and target binding.

To address these shortcomings, the present study combined analysis of serum metabolomics data with verification by western blotting and IHC analysis to improve the accuracy of the results. Based on the aforementioned limitations, future research should aim to conduct molecular docking experiments using the identified active components in MEAG (such as resveratrol and pterostilbene), screen out active monomers that can directly bind to core targets such as MIF and NF-κB and further verify the binding affinity and binding sites between components and targets through *in vitro* technologies, such as surface plasmon resonance and microscale thermophoresis. In addition, *in vitro* cell experiments should be used to clarify the dose-effect association and mechanism of action of single active components or component combinations in regulating the MIF/NF-κB signalling pathway and phenylalanine metabolism, so as to provide further direct experimental evidence for understanding the material basis and structure-activity association of the therapeutic effects of MEAG. Follow-up studies should also aim to construct a positive drug control group with clinically commonly used renoprotective drugs to further determine the therapeutic effect of MEAG on Cis-AKI. In addition, the aforementioned hub targets and key signalling pathways may also serve important roles in Cis-AKI and other kidney diseases, warranting further exploration.

In summary, the present study combined network pharmacology with metabolomics to demonstrate that MEAG improves Cis-AKI by reducing inflammatory reactions and regulating MIF/NF-κB signalling pathway. In addition, serum phenylalanine levels were a key differential metabolite that may be used to evaluate preventative treatment and therapeutic effects. This comprehensive strategy offers a potential

method for identifying the multi-target, multi-pathway pharmacodynamic mechanism of botanical drugs and provided a theoretical basis for the future development of BaiYangJie in clinical practice.

**Acknowledgements**

Not applicable.

**Funding**

The present study was financially supported by the China Academy of Medical Sciences, Medical and Health Science and Technology Innovation Project (grant no. 2021-I2M-1-031), Yunnan Province Wang Jinhui Expert Workstation (grant no. 202405AF140073), Yunnan Science and Technology Talents and Platform Plan (grant no. 202105 AF070011), Yunnan Fundamental Research Projects (grant no. 202201AT070286), the Major Science and Technology Special Plan of Yunnan Province (grant no. 202402AA310041) and the 'Rainforest Talent Support Program' for Young Talents in Xishuangbanna Prefecture (grant no. 2023006).

**Availability of data and materials**

The data generated in the present study may be found in the National Genomics Data Center Open Archive for Miscellaneous Data database under accession number OMIX016002 or at the following URL: (persistent, https://ngdc.cncb.ac.cn/omix/release/OMIX016002).

**Authors' contributions**

BX and GL contributed to the conception and design of the study and drafted the manuscript. LZ and XD contributed to study design, data interpretation and critical revision of the manuscript for important intellectual content. JLC, JS, YL, SL, XZ and TW performed the experiments and contributed to data acquisition and interpretation. JW, DL, XZ and TW performed the network pharmacology and serum metabolomics analyses and contributed to data interpretation. LZ contributed to resources, project administration and funding acquisition. GL and BX confirm the authenticity of all the raw data. All authors revised the manuscript, read and approved the final version, and agree to be accountable for all aspects of the work. GL and BX confirm the authenticity of all the raw data.

**Ethics approval and consent to participate**

All animals were obtained from Sibefu (Beijing) Biotechnology Co., Ltd. The animal research protocol was approved by the Institutional Ethics Review Committee of the Yunnan Branch of the Institute of Medicinal Plant Development, Chinese Academy of Medical Sciences (Jinghong, China; approval no. 20240213001).

**Patient consent for publication**

Not applicable.

**Competing interests**

The authors declare that they have no competing interests.

**Use of artificial intelligence tools**

During the preparation of this work, artificial intelligence tools were used to improve the readability and language of the manuscript or to generate images, and subsequently, the authors revised and edited the content produced by the artificial intelligence tools as necessary, taking full responsibility for the ultimate content of the present manuscript.

**References**

1. Ostermann M, Lumlertgul N, Jeong R, See E, Joannidis M and James M: Acute kidney injury. Lancet 405: 241-256, 2025.
2. Scholz H, Boivin FJ, Schmidt-Ott KM, Bachmann S, Eckardt KU, Scholl UI and Persson PB: Kidney physiology and susceptibility to acute kidney injury: Implications for renoprotection. Nat Rev Nephrol 17: 335-349, 2021.
3. Susantitaphong P, Cruz DN, Cerda J, Abulfaraj M, Alqahtani F, Koulouridis I and Jaber BL; Acute Kidney Injury Advisory Group of the American Society of Nephrology: World incidence of AKI: A meta-Analysis. Clin J Am Soc Nephro 8: 1482-1493, 2013.
4. Dasari S and Tchounwou PB: Cisplatin in cancer therapy: Molecular mechanisms of action. Eur J Pharmacol 740: 364-378, 2014.
5. Motwani SS, Kaur SS and Kitchlu A: Cisplatin nephrotoxicity: Novel insights into mechanisms and preventative strategies. Semin Nephrol 42: 151341, 2022.
6. Ambe K, Aoki Y, Murashima M, Wachino C, Deki Y, Ieda M, Kondo M, Furukawa-Hibi Y, Kimura K, Hamano T and Tohkin M: Prediction of cisplatin-induced acute kidney injury using an interpretable machine learning model and electronic medical record information. Clin Transl Sci 18: e70115, 2025.
7. Ghosh S: Cisplatin: The first metal based anticancer drug. Bioorg Chem 88: 102925, 2019.
8. Fang CY, Lou DY, Zhou LQ, Wang JC, Yang B, He QJ, Wang JJ and Weng QJ: Natural products: Potential treatments for cisplatin-induced nephrotoxicity. Acta Pharmacol Sin 42: 1951-1969, 2021.
9. Zhang X, Chen W, Du Y, Su P, Qiu Y, Ning J and Liu M: Phytochemistry and pharmacological activities of *Arundina graminifolia* (D.Don) Hochr. And other common Orchidaceae medicinal plants. J Ethnopharmacol 276: 114143, 2021.
10. Li J, Zhou L, Wang J, Zhang L, Xia B, Li G, Ren J and Li J: Evaluation of the methanol extract of BaiYangJie: Toxicology and protective effect against acute kidney injury. J Adv Pharm Technol Res 15: 185-193, 2024.
11. Newgard CB: Metabolomics and metabolic diseases: Where do we stand? Cell Metab 25: 43-56, 2017.
12. Cao H, Zhang A, Zhang H, Sun H and Wang X: The application of metabolomics in traditional Chinese medicine opens up a dialogue between Chinese and Western medicine. Phytother Res 29: 159-166, 2015.
13. National Research Council, Division on Earth and Life Studies, Institute for Laboratory Animal Research, Committee for the Update of the Guide for the Guide for the Care and Use of Laboratory Animals: Eighth edition. Guide for the care and use of laboratory animals. National Academies Press, 2011.
14. Shannon P, Markiel A, Ozier O, Baliga NS, Wang JT, Ramage D, Amin N, Schwikowski B and Ideker T: Cytoscape: A software environment for integrated models of biomolecular interaction networks. Genome Res 13: 2498-2504, 2003.
15. Ashburner M, Ball CA, Blake JA, Botstein D, Butler H, Cherry JM, Davis AP, Dolinski K, Dwight SS, Eppig JT, *et al*: Gene ontology: Tool for the unification of biology. The gene ontology consortium. Nat Genet 25: 25-29, 2000.
16. The Gene Ontology Consortium: The gene ontology resource: 20 years and still GOing strong. Nucleic Acids Res 47 (D1): D330-D338, 2019.

17. Tsugawa H, Cajka T, Kind T, Ma Y, Higgins B, Ikeda K, Kanazawa M, VanderGheynst J, Fiehn O and Arita M: MS-DIAL: Data-independent MS/MS deconvolution for comprehensive metabolome analysis. Nat Methods 12: 523-526, 2015.
18. Yan ZH, Li WS, Liang BY, *et al*: Comparison of chemical constituents between Isatidis Radix and Isatidis Folium based on UPLC-Q-TOF-MS/MS technology. Chin Tradit Herbal Drugs 55: 3956-3965, 2024.
19. Meng XW, Cai DJ, Zhu Q, *et al*: Rapid identification of chemical constituents in Dalbergia cochinchinensis heartwood based on UPLC-Q-TOF-MS/MS technology. Chin J Exp Tradit Med Formula 26: 143-156, 2020.
20. Wang YC, Han B, Li ZJ, *et al*: Study on chemical constituents of Dendrobium pendulum based on UPLC-Q-TOF-MS. Chin Pharm J 56: 708-714, 2021.
21. Mou Y, Liu B, Zhang X, *et al*: Component analysis and anti-inflammatory activity evaluation of different parts of Forsythia suspensa based on UPLC-Q-TOF-MS. China J Chin Mater Med 49: 968-980, 2024.
22. Huo JH, Sun GD, Wei WF, *et al*: Analysis of chemical constituents in Niuhuang Qinggan Capsules by UPLC-Q-TOF/MS. Chin Tradit Pat Med 40: 2340-2348, 2018.
23. Lei JC, Zhang ST, Hu XR, *et al*: Investigation of the pharmacodynamic material basis and mechanism of Jinbei Oral Liquid against idiopathic pulmonary fibrosis by UHPLC-Q-TOF-MS/MS combined with network pharmacology. China J Chin Mater Med: 1-16, 2025.
24. Wu CH, Liu YY, Xing SP, *et al*: Screening of potential anti-inflammatory active components of Gonglaomu based on UPLC-Q-TOF-MS metabolomics technology. J Chin Med Mater 48: 389-395, 2025.
25. Kanehisa M and Goto S: KEGG: Kyoto encyclopedia of genes and genomes. Nucleic Acids Res 28: 27-30, 2000.
26. Hayden MS, West AP and Ghosh S: NF-kappaB and the immune response. Oncogene 25: 6758-6780, 2006.
27. Zhang Y, Tang PM, Niu Y, García Córdoba CA, Huang XR, Yu C and Lan HY: Long non-coding RNA LRNA9884 promotes acute kidney injury via regulating NF-kB-mediated transcriptional activation of MIF. Front Physiol 11: 590027, 2020.
28. Chen J, Xu X, Cai Y, Zhang Q, Wang X and Zhang D: Acute kidney injury over the past decade: From definition evolution to pathogenesis insights and innovative therapeutic strategies. Cell Mol Life Sci 83: 156, 2026.
29. Gao J, Deng Q, Yu J, Wang C and Wei W: Role of renal tubular epithelial cells and macrophages in cisplatin-induced acute renal injury. Life Sci 339: 122450-122450, 2024.
30. Megyesi J, Safirstein RL and Price PM: Induction of p21WAF1/CIP1/SDI1 in kidney tubule cells affects the course of cisplatin-induced acute renal failure. J Clin Invest 101: 777-782, 1998.
31. Holditch SJ, Brown CN, Lombardi AM, Nguyen KN and Edelstein CL: Recent advances in models, mechanisms, biomarkers, and interventions in cisplatin-induced acute kidney injury. Int J Mol Sci 20: 3011, 2019.
32. Salei N, Rambichler S, Salvermoser J, Papaioannou NE, Schuchert R, Pakalniškytė D, Li N, Marschner JA, Lichtnekert J, Stremmel C, *et al*: The kidney contains ontogenetically distinct dendritic cell and macrophage subtypes throughout development that differ in their inflammatory properties. J Am Soc Nephrol 31: 257-278, 2020.
33. Ramesh G and Reeves WB: TNF-alpha mediates chemokine and cytokine expression and renal injury in cisplatin nephrotoxicity. J Clin Invest 110: 835-842, 2002.
34. Pober JS: Endothelial activation: Intracellular signaling pathways. Arthritis Res 4 (Suppl 3): S109-S116, 2002.
35. Zhang J, Luan ZL, Huo XK, Zhang M, Morisseau C, Sun CP, Hammock BD and Ma XC: Direct targeting of sEH with alisol B alleviated the apoptosis, inflammation, and oxidative stress in cisplatin-induced acute kidney injury. Int J Biol Sci 19: 294-310, 2023.
36. Zhou X, Jiang K, Luo H, Wu C, Yu W and Cheng F: Novel lncRNA XLOC_032768 alleviates cisplatin-induced apoptosis and inflammatory response of renal tubular epithelial cells through TNF-α. Int Immunopharmacol 83: 106472, 2020.
37. Qu X, Gao H, Sun J, Tao L, Zhang Y, Zhai J, Song Y, Hu T and Li Z: Identification of key metabolites during cisplatin-induced acute kidney injury using an HPLC-TOF/MS-based non-targeted urine and kidney metabolomics approach in rats. Toxicology 431: 152366, 2020.
38. Mahmod II, Ismail IS, Alitheen NB, Normi YM, Abas F, Khatib A, Rudiyanto and Latip J: NMR and LCMS analytical platforms exhibited the nephroprotective effect of Clinacanthus nutans in cisplatin-induced nephrotoxicity in the in vitro condition. BMC Complement Med Ther 20: 320, 2020.
39. Sun J, Shannon M, Ando Y, Schnackenberg LK, Khan NA, Portilla D and Beger RD: Serum metabolomic profiles from patients with acute kidney injury: A pilot study. J Chromatogr B Analyt Technol Biomed Life Sci 893-894: 107-113, 2012.
40. Huang SS, Lin JY, Chen WS, Liu MH, Cheng CW, Cheng ML and Wang CH: Phenylalanine- and leucine-defined metabolic types identify high mortality risk in patients with severe infection. Int J Infect Dis 85: 143-149, 2019.
41. Song Y, Hu T, Gao H, Zhai J, Gong J, Zhang Y, Tao L, Sun J, Li Z and Qu X: Altered metabolic profiles and biomarkers associated with astragaloside IV-mediated protection against cisplatin-induced acute kidney injury in rats: An HPLC-TOF/MS-based untargeted metabolomics study. Biochem Pharmacol 183: 114299, 2021.
42. Ashe K, Kelso W, Farrand S, Panetta J, Fazio T, De Jong G and Walterfang M: Psychiatric and cognitive aspects of phenylketonuria: The limitations of diet and promise of new treatments. Front Psychiatry 10: 561, 2019.
43. Zheng T, Su S, Dai X, Zhang L, Duan JA and Ou-Yang Z: Metabolomic analysis of biochemical changes in the serum and urine of freund's Adjuvant-Induced arthritis in rats after treatment with silkworm excrement. Molecules 23: 1490, 2018.
44. Tokuno M, Commey KL, Yamamoto A, Tokushige M, Tsukigawa K, Nishi K, Otagiri M, Ekino K and Yamasaki K: Insights into the renal protective effects of 7-phenylheptanoic acid in chronic kidney disease mice: Modulation of indoxyl sulfate production and gut microbiome homeostasis. Drug Metab Dispos 53: 100149, 2025.
45. Wang SY and Nesheim MC: Kidney clearance of D- and L-tryptophan by rats. Comp Biochem Physiol A Comp Physiol 85: 451-453, 1986.
46. Gao J, Gu Z, Li M, Xu Y, Gao Y, Wei J, Liang B and Na Y: L-carnitine ameliorates the decrease of aquaporin 2 levels in rats with cisplatin-induced kidney injury. Nephron 135: 315-325, 2017.
47. Chisty TTE, Sarif S, Jahan I, Ismail IN, Chowdhury FI, Siddiqua S, Yasmin T, Islam MN, Khan F, Subhan N and Alam MA: Protective effects of l-carnitine on isoprenaline-induced heart and kidney dysfunctions: Modulation of inflammation and oxidative stress-related gene expression in rats. Heliyon 10: e25057, 2024.
48. Li AS, Baker PR II, Park S, Budnick I, He Z, Okamura K, Gil HW, Miyazaki M, Anderson CC, Reisz JA and Faubel S: Metabolomic assessment reveals depletion of amino acids and energy metabolites in skeletal muscle after ischemic acute kidney injury in mice. Sci Rep 16: 8823, 2026.
49. Okamoto K, Kitaichi F, Saito Y, Ueda H, Narumi K, Furugen A and Kobayashi M: Antioxidant effect of ascorbic acid against cisplatin-induced nephrotoxicity and P-glycoprotein expression in rats. Eur J Pharmacol 909: 174395, 2021.
50. Wei T, Liu B, Chen Y and Li C: Protective effect of ascorbic acid against renal injury induced by 3-chloropropane-1,2-diol-dipalmitate in rats. Renal Fail 46: 2429694, 2024.
51. Kim IY, Song SH, Seong EY, Lee DW, Bae SS and Lee SB: Akt1 is involved in renal fibrosis and tubular apoptosis in a murine model of acute kidney injury-to-chronic kidney disease transition. Exp Cell Res 424: 113509, 2023.
52. Lucas RM, Luo L and Stow JL: ERK1/2 in immune signalling. Biochem Soc Trans 50: 1341-1352, 2022.
53. Capolongo G, Suzumoto Y, D'Acierno M, Simeoni M, Capasso G and Zacchia M: ERK1,2 signalling pathway along the nephron and its role in acid-base and electrolytes balance. Int J Mol Sci 20: 4153, 2019.
54. Poh AR, Love CG, Chisanga D, Steer JH, Baloyan D, Chopin M, Nutt S, Rautela J, Huntington ND, Etemadi N, *et al*: Therapeutic inhibition of the SRC-kinase HCK facilitates T cell tumor infiltration and improves response to immunotherapy. Sci Adv 8: eabl7882, 2022.
55. Sumaiya K, Langford D, Natarajaseenivasan K and Shanmughapriya S: Macrophage migration inhibitory factor (MIF): A multifaceted cytokine regulated by genetic and physiological strategies. Pharmacol Ther 233: 108024, 2022.
56. Bloom BR and Bennett B: Mechanism of a reaction in vitro associated with delayed-type hypersensitivity. Science 153: 80-82, 1966.
57. Lan HY: Role of macrophage migration inhibition factor in kidney disease. Nephron Exp Nephrol 109: e79-e83, 2008.

58. Kong YZ, Chen Q and Lan HY: Macrophage migration inhibitory factor (MIF) as a stress molecule in renal inflammation. Int J Mol Sci 23: 4908, 2022.
59. Pohl J, Hendgen-Cotta UB, Stock P, Luedike P and Rassaf T: Elevated MIF-2 levels predict mortality in critically ill patients. J Crit Care 40: 52-57, 2017.
60. Hoffmann A: Immune response signaling: Combinatorial and dynamic control. Trends Immunol 37: 570-572, 2016.
61. Liu H, Lo CR and Czaja MJ: NF-kappaB inhibition sensitizes hepatocytes to TNF-induced apoptosis through a sustained activation of JNK and c-Jun. Hepatology 35: 772-778, 2002.
62. Grivennikov S, Karin E, Terzic J, Mucida D, Yu GY, Vallabhapurapu S, Scheller J, Rose-John S, Cheroutre H, Eckmann L and Karin M: IL-6 and Stat3 are required for survival of intestinal epithelial cells and development of colitis-associated cancer. Cancer Cell 15: 103-113, 2009.
63. Zhang H and Sun SC: NF-κB in inflammation and renal diseases. Cell Biosci 5: 63, 2015.
64. Liu H, Xiong J, He T, Xiao T, Li Y, Yu Y, Huang Y, Xu X, Huang Y, Zhang J, *et al*: High uric acid-induced epithelial-mesenchymal transition of renal tubular epithelial cells via the TLR4/NF-kB signaling pathway. Am J Nephrol 46: 333-342, 2017.
65. Zhang B, Zeng M, Wang Y, Li M, Wu Y, Xu R, Zhang Q, Jia J, Huang Y, Zheng X and Feng W: Oleic acid alleviates LPS-induced acute kidney injury by restraining inflammation and oxidative stress via the Ras/MAPKs/PPAR-γ signaling pathway. Phytomedicine 94: 153818, 2022.
66. Hu JC, Song JY, Feng R, Ye ML, Xu H, Lu JY, Zuo HT, Zhao Y, Wang JY, Jin JY, *et al*: Integrated gut microbiota-drug interaction analysis and network pharmacology for the investigation of renal-protective effect of Polygala tenuifolia Willd. Int J Mol Sci 26: 10889, 2025.